Chapter 14
Theoretical Modelling, Analysis and Energy Yield Prediction for Horizontal Axis Wind Turbine Rotors

Vasishta Bhargava Nukala, Rahul Samala, Satya Prasad Maddula, Swamy Naidu Neigapula Venkata, and Chinmaya Prasad Padhy

Abstract In this work, aerodynamic modelling of HAWT rotors and energy yield prediction using power curve are studied. The influence of wake losses and rotor solidity on the performance of HAWT is investigated using blade element momentum theory (BEMT). Empirical corrections to a rotor thrust and induced velocities proposed by Glauert, Buhl and Wilson–Walker were evaluated for various Prandtl tip loss factors and validated with experiment thrust data. For axial induction factor less than 0.5, the maximum thrust coefficient obtained using BEMT varied between 0 and 1. When the axial induction factor exceeded 0.5, the Glauert thrust correction factor showed discontinuity for which standard BEMT is invalid. Power coefficient was evaluated for various rotor lift to drag ratios with a rotor diameter of 36 m. The results demonstrated a 17% increase in power coefficient when lift to drag ratios is increased up to three times for tip speed ratios less than 7. A maximum change of ~50% in the power coefficient is obtained when the blade count is increased from one to three. Power curves for 2 MW machine with a diameter of 95 m at two air densities of 1.225 and 1.115 kg/m^3 showed a maximum power error of 29% at cut in wind speed. Time series of 10-min averaged data showed that nominal power is obtained when the blade pitch angle position varied between 0° and 5°. Bin analysis also revealed that maximum value for power coefficient obtained is 0.43, while thrust coefficient of 0.94 at wind speed of 7.6 m/s. Energy yield for a 2 MW turbine is also predicted based on two parameter Weibull distribution for different scale and shape factors.

V. B. Nukala (✉)
Sreyas Institute of Engineering and Technology, Hyderabad, India
e-mail: vasishtab@gmail.com

R. Samala
Indian Institute of Technology Madras, Chennai, India

S. P. Maddula · C. P. Padhy
GITAM (Deemed to be) University, Hyderabad, India
e-mail: cpadhy@gitam.edu

S. N. N. Venkata
National Institute of Technology, Raipur, Raipur, India

A. K. Bohre et al. (eds.), *Planning of Hybrid Renewable Energy Systems, Electric Vehicles and Microgrid*, Energy Systems in Electrical Engineering,
https://doi.org/10.1007/978-981-19-0979-5_14

Keywords Solidity · Airfoil · Rotor blade · Wake · Tip · Wind speed · HAWT · Power coefficient · Thrust coefficient · Power curve

Nomenclature

BEM	Blade element momentum
TSR	Tip speed ratio
L/D	Lift to drag
RPM	Rotations per minute
MSRD	Measured
STRD.	Standard
WPD	Wind power density
O&M	Operations & maintenance
GW	Gigawatt
MW	Megawatt
LCOE	Levelized cost of energy
RANS	Reynolds Averaged Navier Stokes
HAWT	Horizontal axis wind turbine
NACA	National advisory committee for aeronautics
IEC	International electronical commission
TI	Turbulence intensity
MCP	Measure, correlate, predict
BEMT	Blade element momentum theory
DFIG	Doubly fed induction generator
WS	Wind speed
CFD	Computational fluid dynamics
NREL	National renewable energy laboratory

14.1 Introduction

For growing energy demands of future generations, wind turbines are one of the cleanest and cost-effective source of energy supply among all renewable energy technologies. The cumulative wind power capacity installed globally has increased by more than 100% over the last two decades. Countries like US, Germany, Spain and Denmark have the largest number of cumulative wind power installations totalling nearly 200 GW as of year 2018. Further, in China alone the cumulative wind power capacity installed as of year 2019 has reached 200 GW with average size of installed turbine capacity as 1 MW for onshore applications and 3 MW for offshore wind sites. In India, cumulative installed wind power capacity has reached 35 GW with its largest wind park located in the state of Tamil Nadu. Over the past two decades

improved conversion efficiencies from wind turbines have occurred due to innovations in turbine design, manufacturing technologies as well as operation and maintenance procedures. The annual energy production from a wind turbine or a wind farm array is highly improved due to efficient operation and maintenance practices which contributed to low levelized cost of energy (LCOE) from wind power plants (Bhadra et al. 2010; Bossanyi et al. 2005; Emblemsvag 2020; Goudarzi and Zhu 2013). Latest technology in land-based wind power plants consist of rotors installed on tall towers located 50 to 100 m above ground level, while offshore wind towers are floating structures mounted to a depth of 100 m below sea level. At industrial scale operation, there are two orientations for horizontal axis wind turbine rotors, viz. upwind and downwind. In the upwind orientation, rotor is assembled ahead of the tower structure facing the wind direction. In uniform inflow, the risk of blade striking the tower is low in upwind orientation due to positive tilt angle of rotor in the lift producing blades and experiences no tower shadow. However, in downwind configuration, the rotor assembly is placed behind the tower structure. Due to the presence of tower, aerodynamic wake is formed which causes a velocity deficit and an equivalent to velocity potential. Also, when the rotor is inclined downwind of the uniform free stream, the unsteady flow over the blades is responsible for production of aerodynamic noise. This flow also causes increased fatigue loads on structural components of turbine. Although rotor loading influences the turbine efficiency, increase in tip losses contribute to high aerodynamic power loss and is considered an important subject of study by many researchers in wind energy.

Horizontal axis wind turbines are also classified according to pitch and stall control, variable and constant speed types. Machines that utilize the stall phenomenon over the blades to control the power output are considered cost effective than pitch regulated machines. In contrast, pitch operated machines use the blade pitch mechanism powered by induction motors to rotate the blades and orient them into direction of wind. As of year 2019, nearly 70% of turbines installed in the world constitute fixed speed stall-controlled category. The electricity from a wind power plant is regulated using a suitable blade inclination sometimes referred to as pitch angle as well as angular speed of rotor. The blades of turbine rotor are subjected to unsteady aerodynamic and cyclical gravitational force acting on components in nacelle and tower structure due to periodic rotations of blade. For a typical wind turbine, efficiency can be described using its power curve (Snel and Schepers 1995; Vermeer et al. 2003; Directory of Indian Wind Power 2012). The efficiency of turbine varies with thrust (C_T), torque (C_t) and power (C_p) coefficients as well as due to the rotor solidity, blade length, rotational speed and controller algorithms (Jiang et al. 2012; Bhargava et al. 2020; Krishna et al. 2018). Tip loss is considered important when turbine operates in a wind farm array since wakes produced by rotating blade cause a velocity deficit for neighbouring turbine and affect the power production significantly. The Prandtl tip loss factor provides a detailed understanding of dynamics of the wake produced by rotating turbine blade which includes blade count as well as the velocity deficit downstream of turbine. The C_p also known as mechanical power coefficient is evaluated using a coupled form of 1D momentum and blade element theories. Most common theories, viz. generalized momentum theory, blade element

and lifting surface or actuator disc theory that were developed in the past and extension of those theories by using corrections show a profound improvement of thrust and torque prediction on the turbines and propellers.

Shen et al. (2005) analyzed tip loss corrections based on Prandtl (1935) and Glauert (1948) propositions that wake expansion behind turbine rotor is proportional to bound circulation along the blade span. It is known that bound circulation has finite strength and is dependent on lift force acting on blade, density of fluid and free stream velocity. The force coefficients and blade loads are represented by body forces acting on rotor in 3D flow field. They found an approximation of bound circulation as zero towards the tip region led to erroneous results in estimation of induced velocity in axial and tangential directions even for low solidity rotors and at low tip speed ratios. Hence, improved tip corrections to predict the flow field near the blade tip were proposed by Shen et al. (2005) and Mikkelsen et al. (2009) to study the rotor blade loading using combined RANS solver and actuator line solution method (Mikkelsen et al. 2009). This method eliminated Glauert thrust correction for 2D and 3D flow fields since it was able to resolve the turbulent eddies or vortices at the tip region completely, and hence predicted mechanical loads on rotor plane and wake effects on downstream turbines accurately. Similarly, Wilson and Lissamon also proposed empirical thrust coefficient corrections based on the Prandtl tip loss model which assumes the orthogonal nature of the axial induced and relative velocity (Sherry et al. 2013; Shen et al. 2005).

De Vries (1979) showed that orthogonal condition between the axial induced velocity and relative velocity at individual blade element do not yield physically possible flows behind the turbine rotor (Vries 1979). He suggested higher order tip loss corrections which are more realistic and were based on the axial and tangential interference factors similar to that proposed by Prandtl (1935). Similarly, Shen et al. 2005 new tip loss model has also shown that correction of airfoil data towards the tip region is necessary due to the 3D rotational effects of rotor. Improved force coefficients were derived using exponential function of tip speed ratio and blade count. This formulation was applicable to rotors consisting of symmetric and cambered airfoils. Shen et al. 2005 tip correction model was applied on NREL Phase VI experiment rotor blades with S809 airfoil and Swedish WG 500 rotor with blade radius of 5.03 and 2.67 m. It must be noted that orthogonal condition between axial induced velocity and relative velocity was not satisfied when the boundary layer or pressure drag is dominant or included in blade element momentum (BEM) computations. The results from Shen's tip correction model demonstrated better aerodynamic loading in tip region of blade for wide range of tip speed ratios.

Javaherchi et al. (2014) investigated the computational wake modelling around horizontal axis wind turbine (HAWT) rotors using a combination of classical BEM and actuator disc theory based on the fixed and rotating reference frame methods. Although experiment studies and classical BEM theories provide realistic behaviour of wake dynamics to assess the performance of wind turbines, implementation of high-order turbulence models of computation fluid dynamics (CFD) were found more accurate and complemented the experiment data to establish the fidelity of results. Results of CFD simulation tools such as 3D Reynolds averaged Navier Stokes

(RANS) model for axisymmetric flows for modelling of wind turbine wake dynamics agreed well for wide range of tip speed ratios in contrast to BEM and actuator disc theories.

Bontempo and Manna (2019) investigated on errors in axial momentum theory applied to uniform loading of rotors relevant for turbofans' axial flow propellers without wake rotation. In this prediction of pressure and velocity field characteristics, panel methods, lifting line and lifting surface theories have been used. Further 1D axial momentum theory proposed by Glauert (1948) was applied to marine or aerodynamic propellers to examine the tip singularities to investigate unrealistic flows that occur during the wake expansion of rotor (Glauert 1948; Bontempo and Manna 2019; Javaherchi et al. 2014). For steady inviscid incompressible flow assumptions, it is known that generalized momentum theory does not take account of wake rotation; Bontempo noticed that for uniform loaded propellers the axial flow velocity at the tip produced significant errors and hence used combined axial momentum and CFD turbulence model for assessing the flow field near tip region of propeller blades. He also studied the vortex ring method proposed by Oye and improved the BEM model by superposition of ring vortices to predict the axial flow velocity at tip more accurately.

It must be noted that free ring vortex model is based on Kutta–Jukouwski theorem, which is essentially related to bound circulation that is responsible for producing lift forces on annular blade sections (Djojodihardjo et al. 2013). For uniformly loaded propellers, unsteady lift forces produced vortex flux behind the trailing edge of rotor that are assumed to originate from blade root or hub section. In contrast to trailing edge vortex, bound vortex is confined to annular blade section till the pressure gradient within boundary layer cause centrifugal pumping force action in radial direction that was enough to create the helicoidal wake structure downstream of the rotor. Further, he verified that induced velocity also varied predominantly in radial direction but remained constant when the axial thrust coefficient is less than 1.

In another study by Ouikke and Arbaoui (2020), corrections were applied to conventional axisymmetric 1D momentum theory using improved BEM model based on rotor-induced velocities and angle of attack. Experiments on NREL Phase VI rotor were performed to predict the blade loading near the outboard region which takes account of centrifugal and Coriolis forces along radial flow directions. Closed form system of equations was derived, and computer simulations were performed for low solidity wind turbine rotors at moderate tip speed ratios. The new BEM model used iterative methods which also included improved stall delay and 3D rotational augmentation effects in far wake based on the Kutta–Jukouwski theorem. As opposed to classical BEM, this iterative method incurred low computational cost per time step as well as reduced the uncertainty in predicting the aerodynamic forces and induced velocities at tip region of blade (Ouakki and Arbaoui 2020; Sebastian et al. 2019).

This paper is outlined as follows. In Sect. 14.2, a broad classification of horizontal axis wind turbine based on turbine parameters is presented along with historic overview of windmill development. In Sect. 14.3, we describe the geometric model and fundamental aerodynamic principle of HAWT rotors. In Sect. 14.4, aerodynamic force modelling on wind turbine blades is described using blade element momentum

theory. In Sect. 14.5 a pseudocode which can be used to derive the power curve using manufacturer supplied power data is presented. In Sect. 14.6 a mathematical relation between scale and shape factor is derived for predicting annual energy yield at a given location. In Sect. 14.7, results are presented highlighting effects of rotor solidity and tip loss factors on aerodynamic performance based on BEM theory. The combined tip and hub losses for HAWT rotors are calculated for different rotor solidities. Thrust coefficient corrections proposed by Glauert, Buhl, and Wilson–Walker were also computed and validated with the experiment data. The energy yield prediction based on machine power curves is done using two-parameter Weibull distribution. The energy yield is estimated for two different air densities, and reasons for difference in energy yields for varying scale and shape factors is discussed. Time history of 10-min averaged data for electric power, main shaft torque and wind speed are illustrated for pitch-controlled turbine. Finally, in Sect. 14.8 conclusions are presented based on the methods studied.

14.2 Classification of Wind Turbines

Figure 14.1a depicts a chart which shows a broad classification of wind turbine types based on several technology parameters. They include rotation axis, number of blades, rotor orientation, generator technology, speed regulation, power converter, foundation, power regulation, drive train technology and tower structures. Figure 14.1b shows the various types of windmills that have been used over the centuries. Modern wind turbines consist of several components and the blades are critical components that undergo millions of revolutions in its lifetime and experience highly unsteady aerodynamic forces during operation which may often lead to structural component failures of turbine.

14.3 Geometric Model and Aerodynamic Principle of Wind Turbine Rotor

The efficiency of a turbine is dependent upon the geometry of airfoil profiles used for the blade. An airfoil has typically the following important geometrical parameters which affect the efficiency of a turbine blade, viz. chord, thickness, camber and solidity. These properties influence the lift coefficient across the blade span which is responsible for producing the torque of a turbine (Emblemsvag 2020; Directory of Indian Wind Power 2012). Also, at a wind velocity, the force coefficients such as lift and drag on a blade influence the power output from turbine. The solidity is related to the blade element chord at a given span-wise station and expressed as area of plan to swept area of blade section.

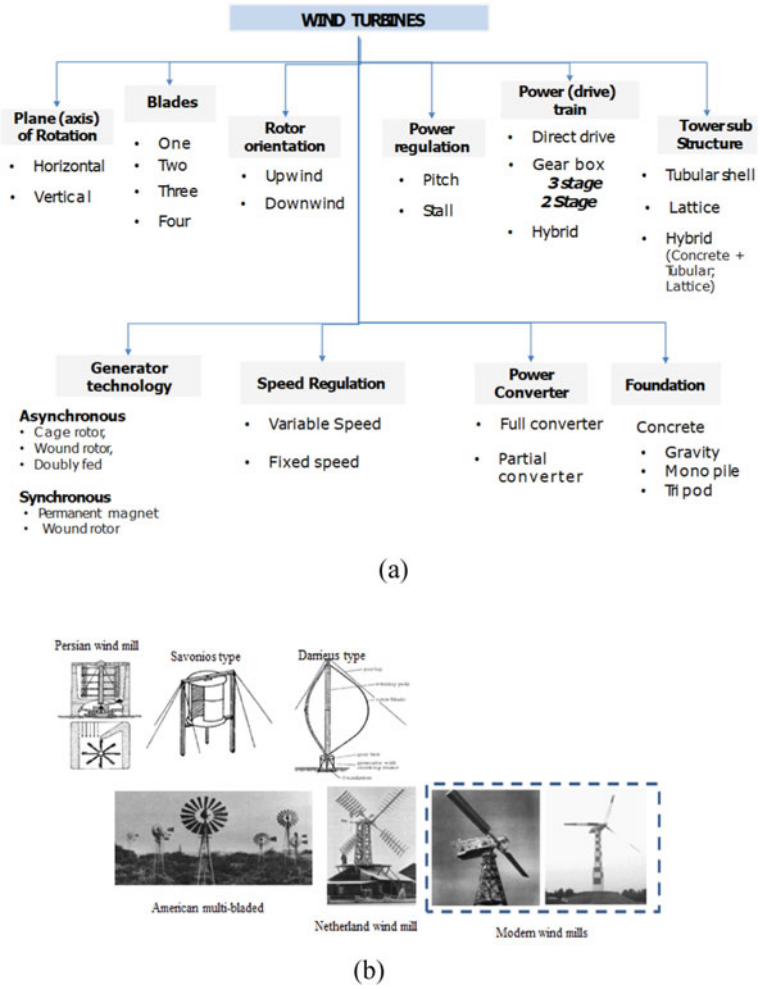

Fig. 14.1 Chart of wind turbine classification based on **a** several turbine technologies, **b** historic snapshots of windmill development over ancient, medieval and modern times (Gasch and Twele 2012)

Figure 14.2a shows the top view of blade element and forces acting on it. From the rotation plane it can be seen that lift (L) and drag (D) forces act along mutually perpendicular directions. Similarly, the normal (F_n) and tangential (F_t) forces are orthogonal to each other. The normal force is oriented out of rotor plane and inclined to the apparent wind speed. The tangential force acts in the rotor plane obtained after resolving lift and drag forces on the blade element and responsible for producing torque in horizontal axis wind turbine rotors. For airfoils with finite trailing edge thickness, the angle of incidence α is angle between the chord line and relative inflow velocity in the direction of fluid motion. The thickness of such an airfoil

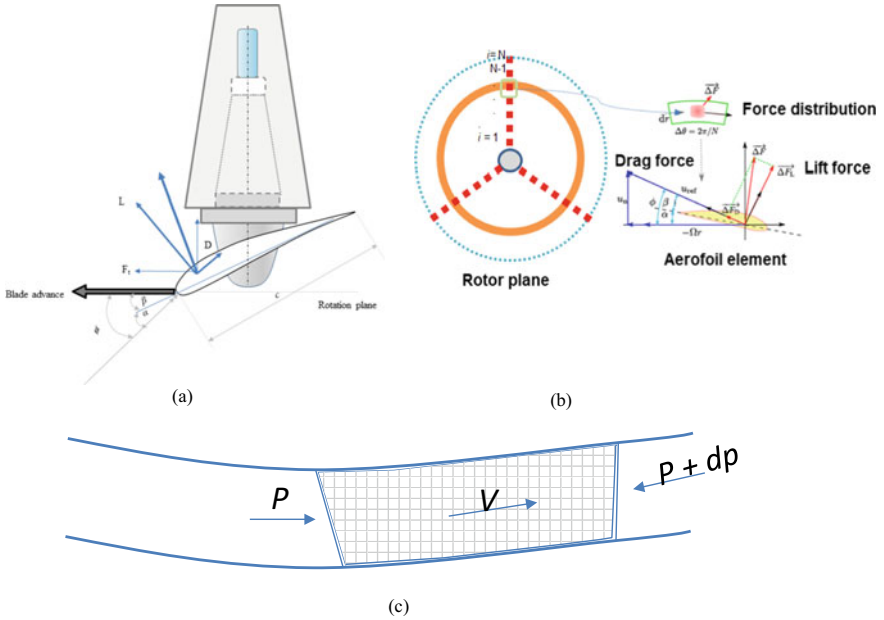

Fig. 14.2 Blade element and forces acting on airfoil of a wind turbine blade **a** top view (adapted from El-Okda (2015)), **b** front view, **c** illustration of stream tube and differential pressure acting on control volume of a fluid element

can be obtained by taking straight line distance between the upper (suction) and lower (pressure) surfaces. Figure 14.2b shows the blade element and aerodynamic forces responsible for producing lift and drag on a rotating airfoil. As mentioned, the lift and drag resulting forces act along mutually perpendicular directions and are inclined at angle of ϕ with respect to apparent wind speed. To considerable extent, aerodynamic power extraction from the wind is attributed to geometric properties shown in Table 14.1. Near blade root, the chord and twist angle for both blades are high and decrease towards the outboard region. The higher twist and chord provide a necessary starting torque required for the turbine. In addition, structural properties such as flexure and torsional stiffness of blade and tower components determine dynamic stability, using natural frequencies and mode shapes of turbine. Table 14.1 shows the geometric properties of blade lengths of 17 and 47 m found common in wind turbine industry. In the present work, BEM analysis has been performed on turbine with blade length of 17 m, while the power curve and energy yield analysis were done for turbine with blade length of 47 m.

Figure 14.2c shows the fluid flow as a stream tube relating pressure and velocity in a finite cross-sectional area. The shaded area represents the control volume for flow field within a stream tube. According to Bernoulli's equation for steady incompressible flows, the pressure differential or pressure head along the streamlines defining the control volume must remain constant (Glauert 1948). This pressure differential for

Table 14.1 Geometric properties of rotor blades of lengths 17 and 47 m

Blade length: 17 m				Blade length: 47 m			
Sl. No.	r/R (–)	Chord, (m)	Twist (deg)	Sl. No.	r/R (–)	Chord (m)	Twist (deg)
1	0.2	1.085	15	1	0.2	3.99	11.1
2	0.25	1.045	12.1	2	0.25	3.9014	10.7803
3	0.3	1.005	9.5	3	0.3	3.6762	9.9358
4	0.35	0.965	7.6	4	0.35	3.454	9.038
5	0.4	0.925	6.1	5	0.4	3.235	8.0833
6	0.45	0.885	4.9	6	0.45	2.9602	7.1666
7	0.5	0.845	3.9	7	0.5	2.6618	6.2659
8	0.55	0.805	3.1	8	0.55	2.4991	5.4173
9	0.6	0.765	2.4	9	0.6	2.348	4.5814
10	0.65	0.725	1.9	10	0.65	2.2016	3.7932
11	0.7	0.685	1.5	11	0.7	2.0419	3.0478
12	0.75	0.645	1.2	12	0.75	1.86	2.3739
13	0.8	0.605	0.9	13	0.8	1.75	1.7
14	0.85	0.565	0.6	14	0.85	1.5601	1.0853
15	0.9	0.525	0.4	15	0.9	1.3688	0.5101
16	0.95	0.485	0.2	16	0.95	1.171	0.1306
17	0.99	0.445	0	17	0.99	0.715	3.0625

a given control volume is a main factor responsible for lift generation on the blades. Figure 14.3a depicts the geometric model of wind turbine rotor with an annular blade section width, *dr*, located at a distance of *r* from the hub center. An increase in effective blade length in a rotor, as well as chord length, tends to increase the rotor solidity. Figure 14.3b demonstrates the rotor disk with finite solidity. Figure 14.3b also shows that an increase of blade count from two to three changes the rotor solidity by factor of 1.7. The blue color line shows the solidity factor for three blades and red line for two blades. Evidently, the solidity factor continues to increase near hub where profiles are thick and wide. However, it reduces outboard of span where the chord length becomes appreciably low compared to maximum chord of the blade. Like a wind turbine blade, an aircraft wing also exhibits maximum lift generation along its span for a given incidence angle. The tip vortices that are observed on aircraft wings have finite aspect ratios. As the aspect ratio is increased the maximum lift coefficient on wing is also increased. The formation of tip vortices produces a downwash on the wing that varies with flow angle of attack as well as Reynolds number. Downwash tends to reduce effective lift generated on aircraft wing due to high turbulence and is considered disadvantageous. Therefore, modern high speed aircraft wing tips are bent at an angle inclined to vertical plane. To counter reduced lift, active flow control methods such as suction and blowing are created to produce sufficient momentum and prevent the boundary layer flow separation at moderate to

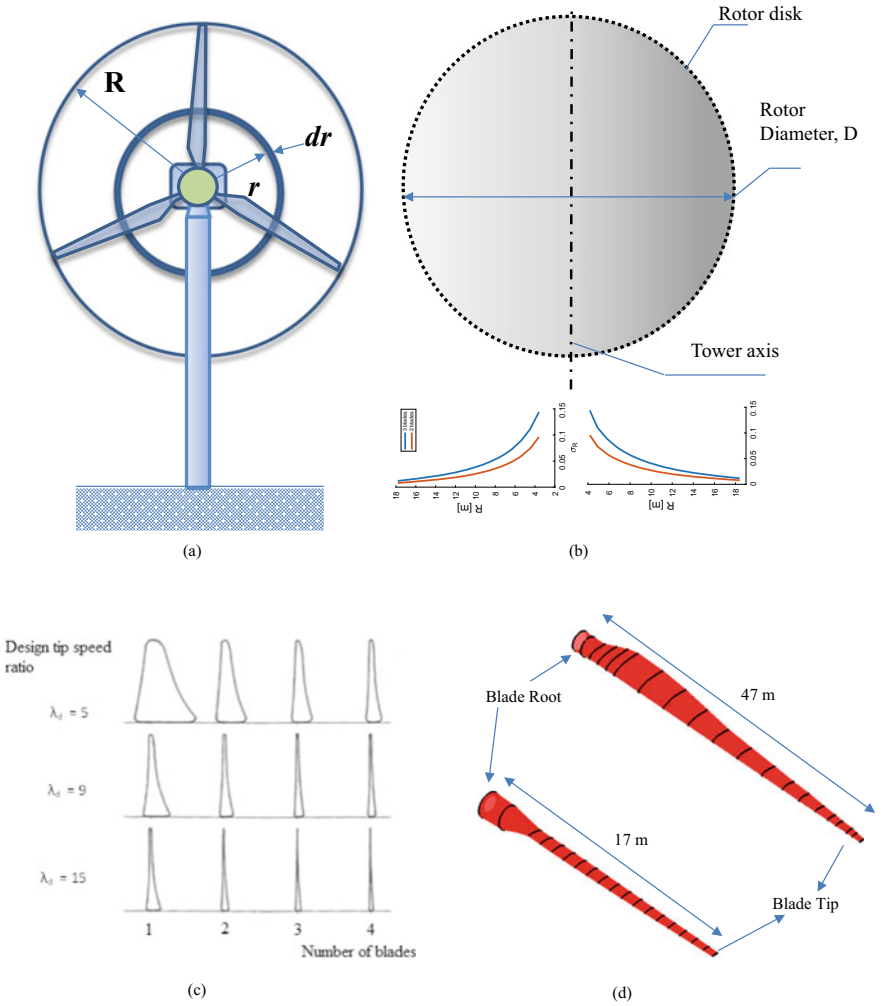

Fig. 14.3 **a** Illustration of annular blade section for three-bladed wind turbine rotor (Bhargava et al. 2020). **b** Comparison of rotor solidity from root to the tip of blade for three- and two-bladed wind turbine rotors. **c** Standard blade plan forms for various design values of λ and blade count (Jordan, et al. 2019). **d** Isometric view of the 17 and 47 m blades used in current study, developed in NuMAD software (https://energy.sandia.gov/programs/renewable-energy/wind-power/rotor-innovation/numerical-manufacturing-and-design-tool-numad/)

high flow angles oriented to wing (Genc et al. 2016). However, commercial use of such techniques has not been used in wind turbine industry till date to improve the aerodynamic efficiency of rotor. For wind turbines, at a given free stream velocity, the axial induction factors at the rotor disc continuously vary according to the inflow angles and the lift and drag forces on the blade. This unsteady nature of lift and drag forces are resolved in axial and tangential directions of rotor plane to produce thrust

Table 14.2 Key turbine parameters

Parameter	Value/Description	
Wind zone	IIA/IIIB	IIIB
Top height	80 m	50 m
Nominal power	2100 kW	500 kW
Diameter of rotor	95 m	36 m
Blade count	3	3
Cone angle	1	0
Tilt angle	3	2
Pitch imbalance	–	0.1°
Mass imbalance	–	–
Airfoils	NACA 63-xxx; FFA-W3-301	NACA 0012, NACA 4412, NACA632xx series
Power regulation	Stall control	Pitch control

and torque coefficients. In general, rotor solidity is given by Eq. (14.1)

$$\sigma = \frac{Nc}{2\pi \frac{r}{R}} \tag{14.1}$$

where N is number of blades; c is local blade chord; r/R is the normalized blade span.

Table 14.2 shows the turbine design parameters along with type of NACA airfoil family used for rotor blades. Aerodynamic data for airfoils are based on wind tunnel tests conducted on 2D sections. Conventional turbine designers relied on airfoil data that were used in aircraft industry which were typically 4-, 5- and 6-digit series, e.g. NACA 230xx, NACA 44xx, NACA 63-2xx. Due to rapid technology changes and adoption of new technologies from aircraft industry, the aerodynamics of blade design used devices such as winglets, flaps and vortex generators has resulted in the continuous increase of maximum lift coefficient and hence improved energy yield from a wind turbine.

Figure 14.3c shows that for a tip speed ratio range, increasing thickness to chord ratio and chord length of the blade reduces the design tip speed ratio. It also renders that for moderate thickness to slender blades the design tip speed ratio is higher and typically range between 9 and 15. According to Ragheb and Ragheb (2011), the theoretically optimum tip speed ratio is inversely proportional to number of blades in turbine and is given by $\lambda = 2\pi/B$ where B is blade count. Higher values of tip speed ratio (TSR) show that blades rotate faster in the wind field and convert more kinetic energy to mechanical energy. However, it must be noted that too low values of TSR explains that blades tend to escape the free wind and hence increase the uncertainty to extract aerodynamic power. Further explanation about the design tip speed ratio is demonstrated in Sect. 14.7.2. Figure 14.3d shows the comparison of the plan form of 17 m and 47 m blade length developed using NuMAD

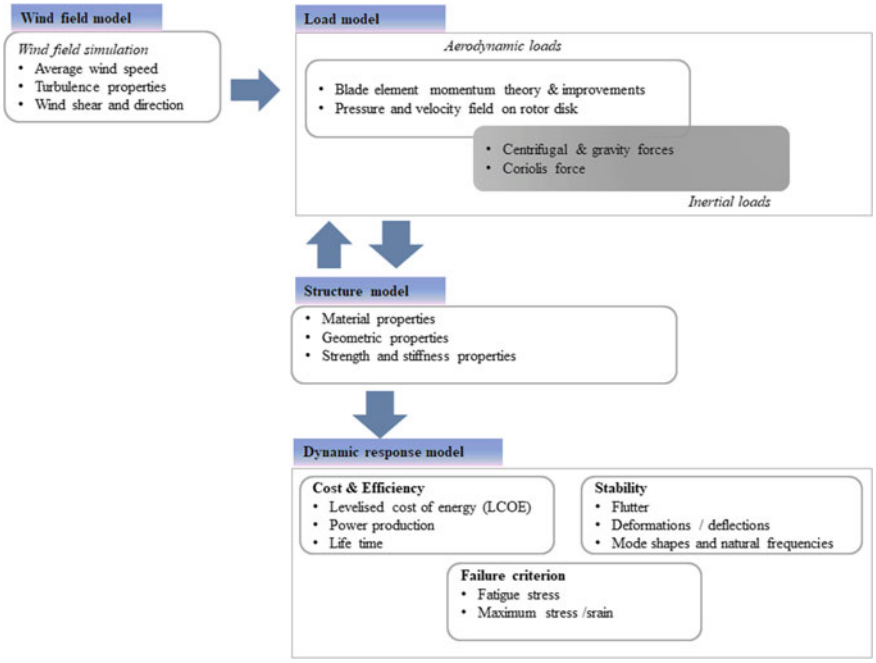

Fig. 14.4 Schematic showing interaction between structural and aerodynamic processes for a HAWT (adapted from Andrew and Flay 1999)

software (https://energy.sandia.gov/programs/renewable-energy/wind-power/rotor-innovation/numerical-manufacturing-and-design-tool-numad/).

Figure 14.4 depicts the aero-elastic response model for a wind turbine system. Modern wind turbine blades are built using composite materials typically made of glass fiber reinforced plastic (GFRP). They are designed to deliver improved mechanical properties such as strength and stiffness at a low weight and cost than conventional materials. The structural model of an aero-elastic system achieves these properties by using sandwich laminates which can be oriented in symmetric or anisotropic manner. By doing so, the geometry of blade is coupled to material characteristics to attain desired bending and torsion stiffness enhancements at various loading modes. It can be said that the response characteristics of an aero-elastic system utilizes the finite element method (FEM) approach and depend on the wind field, loading and structural models. The loading model shown in Fig. 14.4 includes the forces and moments due to aerodynamic, inertial, gravity, centrifugal and operational modes in the chord and span directions of blade.

14.4 Blade Element Momentum (BEM) Theory

The earliest known theoretical model for horizontal axis wind turbines was based on the actuator disk theory conceptualized by Rankine (1865) and Froude (1885) and was originally intended for propellers and helicopters. Actuator disk theory considered wind turbine rotor as stationary solid disk that could extract translational kinetic energy from wind to rotational energy. During this process, a change in momentum occurs and energy extraction is made possible through mechanical devices. Later, Lanchester and Betz proved that maximum possible power that can be extracted from a wind turbine as 59.3%. He essentially utilized the Bernoulli's principle of conservation of energy by assuming that the kinetic energy in wind and pressure drop across the turbine can be converted to useful mechanical work. Prandtl (1918) and Glauert (1935) later redesigned it with significant improvements to the assumptions of basic actuator disk theory. It is renamed as actuator line model which consists of imaginary streamlines in form of tubes that extended upstream and downstream of the rotor disk. The force distribution on lifting surface such as wind turbine blade can be governed by actuator line model. This model was modified by introducing the rotation of wake behind the rotor to find aerodynamic power losses in a reliable manner. This led to the foundation of BEM theory which is discussed in next section.

Lifting line theory was first proposed by Prandtl and Lanchester during World War I and based on assumption that flow around wings of finite span was approximated by discrete summation of flow around the thin airfoil elements of wing. Also, the wing is assumed as flat plate and the nature of flow around each airfoil element is predominantly 2D. It considered the 3D flow behaviour taking account of trailing edge vortex on wingspan which is depicted as helical wake that expands downstream producing downwash on the wing. For uniform flows, the downwash is caused due to bound circulation which varies uniformly along the wingspan. The strength of such bound circulation at arbitrary distance in radial direction can be determined using Biot–Savart law. An important drawback of this theory was that it does not account for thickness distribution, dihedral angle and in-plane sweep angle along span but considers twist and taper. It can be noted that downwash is produced due to tangential-induced velocity along the wingspan causing a trailing edge vortex which expands far downstream of wing. This theory also considers normal induced velocities along wingspan to predict the strength of downwash computed by means of Biot–Savart law. The lift produced is proportional to strength of circulation which is essential to predict the inflow angles and angle of attack. At higher or near stall AOA, higher lift forces and thrust on the wingspan or a rotor blade are expected (Snel and Schepers 1995).

14.4.1 BEM Theory Assumptions and Formulation

From classical BEMT, velocity field on each airfoil having a finite width *dr* is different from remaining airfoils (Bhadra et al. 2010; Emblemsvag 2020). The flow is fundamentally free of any shear forces and constant fluid density along the rotor plane which means no wake trails of fluid rotation are present. Further, wake losses due to tip are not modelled due to rotor being assumed as solid disk (Bhadra et al. 2010; Sherry et al. 2013). No yawing is accounted in BEMT. As mentioned earlier, the limiting value for aerodynamic power extracted by a horizontal axis turbine is 16/27 = ~59.3% which according to Betz is impossible to achieve practically. This limit occurs when the axial induction factor at rotor disk reaches a value of 0.33 (Hansen 2010). In general, the C_p for a turbine containing finite number of blades can be approximated using velocity triangles method. C_p and C_T for machine can be evaluated using below steps for a given L/D ratio

- At every blade section, the inflow angle is computed using Eq. (14.2). The inflow angle at any blade section is function of λ.
- From the inflow angle, the axial induction factor is computed at individual airfoils given by Eq. (14.3.1).
- For a given tip speed ratio, airfoil efficiency and tip loss factor for each blade are integrated to evaluate peak aerodynamic efficiency of rotor.
- For L/D values of 40, 80 and 120, the C_p is given using Eqs. (14.2) and (14.3.1, 14.3.2).

$$\emptyset = \tan^{-1}\left[\frac{1}{\left(\frac{r}{R}\right)\lambda}\right] \tag{14.2}$$

$$a = 4\lambda\mu^2\left[\frac{\sin\left[\frac{2}{3}\emptyset\right]^3}{\sin[\emptyset]^2}\right]d\mu \tag{14.3.1}$$

$$\eta = 1 - \frac{\lambda}{C_l/C_d} \tag{14.3.2}$$

- Prandtl tip correction is expressed as function of blade count, the increase in tip velocity with respect to free stream and inflow angle of blade. The overall turbine efficiency can therefore be evaluated by summing airfoil's efficiency wake loss factor due to tip and wind velocity deficit factors as well as lift to drag ratio along the blade span.
- The ratio of aerodynamic efficiency to the maximum possible efficiency for the assumed lift to drag ratios includes the tip loss factor (Bossanyi et al. 2005; Snel and Schepers 1995; Vermeer et al. 2003).

More detail steps on how to derive power coefficient using velocity triangles are explained later in this section. For smaller turbine conservative ratios of L/D are found to vary commonly in the range 40–60. In actual cases, this will vary up to L/D

= 120, for large megawatt scale wind turbines at high Reynolds number. A large value of L/D ratios means higher C_p for a turbine and implies the exceedance of Betz limit. The Prandtl tip and hub loss factor can be expressed mathematically from Eqs. (14.4) to (14.6)

$$F(\mu) = ft(\mu) \cdot fr(\mu) \tag{14.4}$$

where F is total wake velocity deficit, $f_r(\mu)$ is root wake velocity deficit, $f_t(\mu)$ is tip wake loss factor, μ is the normalized blade radius, r/R, μ_R is normalized blade root radius, N is number of blades, a is axial induction factor at the rotor disc and λ is tip speed ratio

$$f_r(\mu) = \frac{2}{\pi}\cos^{-1}\left[e^{-\left(\frac{N}{2}\right)(\mu-\mu_R)/\mu\sqrt{1+(\lambda\mu)^2/(1-a)^2}}\right] \tag{14.5}$$

$$f_t(\mu) = \frac{2}{\pi}\cos^{-1}\left[e^{-\left(\frac{N}{2}\right)(1-\mu)/\mu\sqrt{1+(\lambda\mu)^2/(1-a)^2}}\right] \tag{14.6}$$

The rotation of blade causes the flow movement in axial, radial and tangential directions. In this process, angular momentum of rotor is not constant and dynamic stall phenomenon occurs at an AOA beyond the critical angle, typically about 16°. For chord-wise direction of blade, near stall angles of attack, flow becomes more turbulent and causes local circulation to expand to the tip of the blade. Similar phenomenon is also observed near center of rotational axis of machine. These vortices cause the aerodynamic power loss at high tip speed ratios which are undesirable. In the current study, only the wake loss from tip is examined (Bossanyi et al. 2005). Wake loss from tip is high for turbines operating in large wind farms due to interaction of wake from neighbouring turbines which causes a velocity reduction and affects the overall power output from a wind farm.

In case of wind turbine rotors, the maximum C_p and C_T during yaw is expressed in terms of yaw angle and given from Eqs. (14.7) to (14.10)

$$C_p = 4a(\cos\gamma - a)2 \tag{14.7}$$

$$a = \frac{\cos\gamma}{3} \tag{14.8}$$

$$C_{p,\max} = \frac{16}{27}(\cos\gamma)^3 \tag{14.9}$$

$$C_T = 4a\sqrt{1 - a(2\cos\gamma - a)} \tag{14.10}$$

γ is the yaw inclination, and a is the velocity deficit factor. In the present study, the maximum power coefficient is evaluated using axial momentum theory which predicts the C_p value better than Glauert's correction to momentum theory. For steady

incompressible aerodynamic flows, actuator disc and BEM theory can be evaluated at all values of axial induction factor. In practice, however, results from BEM theory are not accurate when the axial induction factor exceeds 0.33 but is less than 0.5 (Strangfeld et al. 2015; Hansen 2010). When the value of a crosses 0.5, the BEMT produces invalid or inaccurate loading results for a turbine. Further, Mansberger (2016) derived the blade element theory based on thermodynamic model which states that kinetic energy in the flow field is converted to internal or thermal energy and vice-versa within the control volume (Mansberger 2016). It predicts higher values for C_p for all values of axial induction factor, a compared to Betz limit derived from classic BEMT and claims maximum C_p to be 65.1% when a is 0.457 thus disproving the Betz limit. Also, it assumes that diameter of near wake expands causing an increase in velocity deficit while the diameter of far wake contracts leading to reduced velocity deficit. Although velocity deficit has been proven and validated using laser doppler velocity measurement data the details of this thermodynamic model are beyond the scope of present study.

As mentioned earlier velocity deficit that occurs across the rotor disk can be expressed by Eq. (14.11)

$$a = \frac{U_0 - U_d}{U_0} \tag{14.11}$$

This factor varies on the extent of pressure drop and velocity reduction of free stream air flow downstream of rotor disk. It can be said that axial induction factor a shows large variation when the tip speed ratio of rotor is high. Furthermore, a large velocity deficit produced far downstream of rotor will induce a higher thrust coefficient. This incremental change in thrust coefficient far downstream is an important parameter in the design of wind farms for a given site. However, the resultant velocity seen by blade section located at radius r varies with both axial and angular induction factors and is expressed by Eq. (14.12)

$$W = U_r = \sqrt{\{(U_0(1-a))\}^2 + \{r\Omega(1+a')\}^2} \tag{14.12}$$

It must be noted that axial induction factor according to Eq. (14.3.1) can be rearranged in terms of inflow angle, ϕ and local blade solidity, σ_r, aerodynamic force coefficients, C_l and C_d to yield from Eqs. (14.13) to (14.15), respectively.

$$\emptyset_r = \tan^{-1}\left(\frac{1-a}{(1+a')\lambda_r}\right) \tag{14.13}$$

$$\frac{a}{(1-a)} = \frac{\sigma_r[C_l \cos\emptyset + C_d \sin\emptyset]}{4\sin^2\emptyset} \tag{14.14}$$

$$\frac{a'}{(1+a')} = \frac{\sigma_r[C_l \sin\emptyset - C_d \cos\emptyset]}{4\sin\emptyset\cos\emptyset} \tag{14.15}$$

The change in the lift and drag force vectors on a local chord of an airfoil is given by Eqs. (14.16) and (14.17), while the resolved force components in axial and tangential directions of the rotor plane are given from Eqs. (14.18) to (14.20)

$$dF_L = 0.5\rho U_r^2 c_r C_l dr \tag{14.16}$$

$$dF_D = 0.5\rho U_r^2 c_r C_d dr \tag{14.17}$$

$$dF_N = dF_l \cos\emptyset + dF_d \sin\emptyset \tag{14.18}$$

$$dF_T = dF_l \sin\emptyset - dF_d \cos\emptyset \tag{14.19}$$

$$dM = dT = [dF_l \sin\emptyset - dF_d \cos\emptyset] \cdot r \tag{14.20}$$

During the rotation, a centrifugal pumping action of the airstream tends to occur in radial direction of the rotor disk and is responsible for delaying stall on the blades. The air flow near root or hub rotates in rotation plane and moves towards the tip of blades and flow eventually forms a bound vortex along blade span and tip vortex at tip of blade which is responsible for local lift generation. These vortices are shed in a cyclical manner in the form of a helix which extends downstream of turbine rotor. The differential thrust and torque equations are expressed in terms of total wake loss or deficit factor F and are given by Eqs. (14.21) and (14.22)

$$dA_{\text{Thrust}} = 4\pi\rho a(1-a)U_0^2 \cdot r dr\,\text{F} \tag{14.21}$$

$$dA_{\text{Torque}} = 4\pi\rho r\omega a'(1-a)U_0 \cdot r^2 dr\,\text{F} \tag{14.22}$$

The torque, power and thrust coefficients can be expressed from Eqs. (14.23) to (14.25)

$$C_t = \frac{T}{0.5\rho\pi R^3 V^2} \tag{14.23}$$

$$C_p = \frac{P}{0.5\rho\pi R^2 V^3} \tag{14.24}$$

$$C_T = \frac{F}{0.5\rho\pi R^2 V^2} \tag{14.25}$$

where T is mechanical torque, N-m produced by the main shaft of turbine. R is blade radius, m, V is uniform speed measured in m/s, P is aerodynamic power, kW, ρ is air density in kg/m^3, F is the resultant normal force acting on rotor. A simple algorithm to implement BEM for HAWT rotors consist of following steps.

1. Begin with a and a' as zeros.
2. Compute the blade flow angle relative to apparent velocity field, ϕ.
3. Determine chord angle relative to apparent velocity field, α.
4. Import the C_l (α) and C_d (α) table data.
5. Calculate the force coefficients in axial and tangential directions relative to free stream.
6. Determine the velocity deficit factors in normal and along rotor plane, a and a'.
7. Fix a condition to a and a' for solution stability; otherwise repeat process from step 2.
8. Apply the tip wake loss factors.

14.4.2 Wind Shear Approximation

Wind shear is a measure of gradient in wind speed and it can vary in horizontal and vertical direction in atmosphere. Wind speed in atmosphere can be considered as stochastic and is described using parameters such as turbulence intensity and roughness height. Further mean wind speeds are found to increase with height above ground. For a given geographic location, it is function of orography factors like obstacles, e.g. buildings, trees, vegetation and expressed by reference surface roughness, z_0. The turbulence characteristics of wind field seen by a wind turbine rotor can thus be conveniently expressed in terms of roughness height, z, above the ground and wind shear exponent, ε. For a turbine operating at a windy site, the wind shear approximation can be done either by power law or logarithmic law given by Eq. (14.26) and Eq. (14.27), respectively. For BEM studies, a wind shear exponent of 0.1 for power law in Eq. (14.26) has been assumed which represents the plain or open grass land with few dispersed vegetation.

$$\frac{U(z)}{U_{ref}} = \left(\frac{z}{z_{ref}}\right)^{\varepsilon} \tag{14.26}$$

$$\frac{U(z)}{u_*} = \frac{1}{k}\ln\left(\frac{z}{z_0}\right) \tag{14.27}$$

U is mean wind speed in m/s; u_* is the friction velocity; k is the von-Karman constant, 0.4; z is the height above ground in m; z_0 is the reference surface roughness length in m.

14.4.3 Limitations and Improvements to Classical BEM Theory

As mentioned in the earlier section, BEM is based on 1D linear momentum theory in which a turbine rotor is modelled as uniform disk consisting of finite number of blades with discrete blade elements. It has several limitations since it cannot model complex flows around the rotor and its accuracy varies during stalled and unsteady flow conditions during yaw operation. Also, there is no rotation and expansion of wake downstream of turbine rotor. More advanced aerodynamic models for load modelling are dependent on the wake structure behind the rotor such as the prescribed wake or free wake vortex acceleration potential methods which have been successfully implemented for propeller and helicopter aerodynamics and adapted to HAWT rotors. Simulating 3D non-linear wake structures requires advanced wind turbine design codes based on CFD techniques that are computationally intensive and prohibitive in nature. In the recent past, modern wind turbine design codes have been modified and aimed to improve accuracy by implementing corrections to the standard BEM code by integrating engineering models that take account two important factors, viz. dynamic stall and dynamic wake. In each case, 2D static airfoil profile data is corrected for 3D effects that include tip and hub loss as well as stall delay along the blade span to increase section lift coefficient or limit the blade loading. An empirical stall delay model proposed by Corrigan and Schillings (1994) given by Eqs. (14.31) and (14.32) in Corrigan and Schillings (1994) takes account of vortex wake rotation effects observed at high AOA. It utilizes the trailing edge angle, local radius, local chord length of blade segment and velocity gradient parameter to determine the change in AOA. This model was applied by Tangler and Selig (1997), Xu and Sankar (2002) for determining increment C_L values (Tangler and Selig 1997; Xu and Sankar 2002). Empirical relations often give a useful estimate for verifying the BEM results. A simpler approximation to C_p according to Manwell et al. (2009) is given by Eq. (14.28)

$$C_p = \frac{16}{27}\left[\frac{\lambda B^{0.67}}{1.48 + \left(B^{0.67} - 0.04\right)\lambda + 0.0025\lambda^2} - \left(\frac{1.92\lambda^2 B}{1 + 2\lambda B}\right)\frac{D}{L}\right] \tag{14.28}$$

Another essential approach is the inverse BEM method in which angle of attack (AOA) and inflow angle values are obtained using the blade loading functions. Transfer functions are utilized in the process to determine the inflow angle pattern for different flow conditions; however, such predictions are often difficult to verify limited extensive experimental data and hence a major constraint in BEM theory validation.

14.4.4 Turbulence Intensity and Empirical C_p Model

Turbulence intensity (TI) is an indicator of *randomness* or *gustiness* in wind. It is the ratio of standard deviation of longitudinal value of wind speed component to its magnitude of free stream velocity and is expressed using Eq. (14.29). For wind data obtained at a given location, it is an important parameter which is used for predicting the fatigue life of wind turbine components. Typically estimates for turbulence intensity parameter vary with long-term data and also according to orography properties of a geographic site. According to Germanischer Lloyd wind turbine certification standards, there are broadly two turbulence intensity classes which are termed as *A* and *B* and are equal to 18% and 16%, respectively (Germanisher 2007).

$$TI = \frac{\sigma}{\overline{V}} \tag{14.29}$$

As mentioned in Sect. 14.3, the power regulation for a pitch-controlled turbine changes due to blade angle. The C_p is function of blade pitch angle β and TSR λ. A model proposed by Heier (1998) for double fed induction generator (DFIG) has been analyzed in the present study. In the present study, the power coefficient C_o is given according to empirical exponential formulation using Eqs. (14.30) and (14.31). It can be seen that Eq. (14.30) is dependent on coefficients c_1, c_2, c_3, c_4, c_5 and c_6, blade pitch angle and tip speed ratio of turbine. In the present case, the values for those coefficients have been tested for turbine with 95 m rotor diameter in such a way that power coefficient values remained within 1% of the manufacturer obtained power coefficient.

$$C_p(\lambda, \beta) = c_1\left(\frac{c_2}{\lambda_i} - c_3\beta - c_4\right)e^{-\frac{c_5}{\lambda_i}} + c_6\lambda \tag{14.30}$$

$$\frac{1}{\lambda_i} = \frac{1}{\lambda + 0.08\beta} - \frac{0.035}{\beta^3 + 1} \tag{14.31}$$

14.5 Power Curve Determination

Accurate modelling of power curve is essential to forecast the power output from a single or group of turbines. In the power curve analysis, averaged wind speed and electric power are often essential to estimate energy. Data reduction and corrections are necessary with respect to cut-in and cut-out wind speeds by using the method of bins. A cut-in wind speed is a minimum value at which turbine starts delivering power to grid.

Rated wind speed is a value when the generator produces nominal power. Both cut-in and rated wind speeds are fixed values while a cut-out wind speed is not a

Table 14.3 Pseudo code: wind turbine power performance

STEP 1: Initialize data

PowerData : i ←1 to N // N is data length or samples
ThrustData : i ← 1 to N
TorqueData : i←1 to N
WindSpeedData : i ←1 to N

STEP 2: Assign counters

ThresholdPowerData : = 1 to 25 //set threshold values of electric power corresponding to wind speed
CountWS := 1 to 25 // wind speed bin
k: = 1 // set counter for bin average
i: = 1 // set counter for data increment

STEP 3: Algorithm
WHILE k <= 25, **Do**
FOR i ← 1 to N **Do**
1. Check for wind speed bin limits
IF $WindSpeedData_k >= CountWS_k$ and $WindSpeedData_k <= CountWS_k$ **Do**
$PData_{i,k} := PowerData_{i,k}$ // extract electric power data values
$ThrustData_{i,k} := ThrustData_{i,k}$ // extract thrust data values
$TorqueData_{i,k} := TorqueData_{i,k}$ // extract torque data values
END IF
2. If invalid data is found in extracted bins, replace with empty character
Else Go to 3
3. i ← i+1
END FOR
P_m_k := Do the average of ($PowerData_{i,k}$)
$Thrust\_m_k$:= Do the average of ($ThrustData_{i,k}$)
$Torque\_m_k$:= Do the average of ($TorqueData_{i,k}$)

IF P_m_k < twice $ThresholdPowerData_k$ || P_m_k >= twice $ThresholdPowerData_k$ **Do**
$P\_m_k := P\_m_k \pm$ Standard deviation of $PowerData_{i,k}$ //set standard deviation according to bin count
END IF
k ← k +1
END WHILE

STEP 4: Display outputs

PRINT CountWS, P_m
PRINT CountWS, Thrust_m
PRINT CountWS, Torque_m

STOP

constant. Power hysteresis algorithms are usually implemented by turbine operators for above rated wind speeds in order to reduce loads and extend lifetime of turbine components. For certification of power curve, IEC 61400-12-1 is followed for power performance measurements in case of single turbine. The standards tell about the measurement method for actual power curve determined using time varying values for wind velocity and power at a test site. The typical bin width is taken as 1 m/s for below nominal wind velocity and 2 m/s when wind velocity is above nominal values.

Table 14.3 shows the pseudo code implemented for power curve analysis in the present study. The power curves vary with size of turbine and its manufacturer specifications. Between minimum threshold and nominal values, the curve varies almost linearly in response to the wind speed for both pitch control and stall-controlled turbines. For above rated wind speeds, the power output remains constant for pitch-controlled turbines while it reduces in case of stall-controlled turbine. For any case, bin averaging procedures are applied to measured data. It can be noted that bin averaging of data is necessary for each performance parameter in which data range for each bin needs to be sorted, summed and divided with the total data samples per bin. For some wind speed bins around cut-in values, the bin values for power data appear to be negative. The negative values indicate that generators consume reactive power from grid.

Operational data is acquired through a digital data acquisition system and monitored for accuracy of measured signals which can impact the energy production for given period. The system must ensure that error free data is recorded. This can be achieved by checking the accuracy and linearity of sensors, transducers, and preamplifiers. The minimum sampling rate for measurement is 0.5 Hz according to IEC 61400-12-1 standards. Erroneous data can be measured by anemometer, and when the anemometer is present in the wake can thus be eliminated by following standards and procedures. It can be noted that sensors used to measure electric power data must ensure $\pm 0.5\%$ accuracy of the rated power of wind turbine required for power curve verification (Power performance testing 1990).

Commercial wind farm design tools such as WAsP and Wind Farmer are software which can model the complex flow conditions at given site. They use quantitative methods for forecasting long-term wind speed and consists of measure, correlate and predict (MCP) procedures. MCP is a method to predict long-term wind conditions, i.e. speed and direction at a target site by correlating it with the short-term concurrent or time series measured wind data from a nearby reference mast. To avoid energy losses due to wind farm array design, factors such as inter-turbine spacing, closeness of wind farm electrical infrastructure and orography variables are important. Further, soiling losses that occur due to change in surface roughness of blade can be minimized when best practices in operation and maintenance are followed. Knowing the accuracy of power output from a turbine at a given wind speed provides useful information in the design process of turbine or its components. It is also useful for wind turbine operators and power grid companies to forecast the energy prices and power trading in electricity markets. A flow chart for an iterative numerical prediction algorithm used in data analysis is shown in Fig. 14.5. It must be noted that these factors affect the gross energy output from a wind farm. The data required for energy yield assessment is quantified using power and thrust curves and depends on measured wind velocity data. The quality of measured wind speed data at a site also depends on the distance of met mast to a neighboring turbine. Also, the boom orientation on mast is critical to measuring the wind velocity accurately. The number of velocity sensors mounted on mast and hysteresis of wind vane error also contributes to uncertainty in power productions from a wind farm (Astolfi et al. 2020). Direction measurement must be accurate within $\pm 3^{\circ}$. According to Garrad Hassan sensor errors contribute to nearly

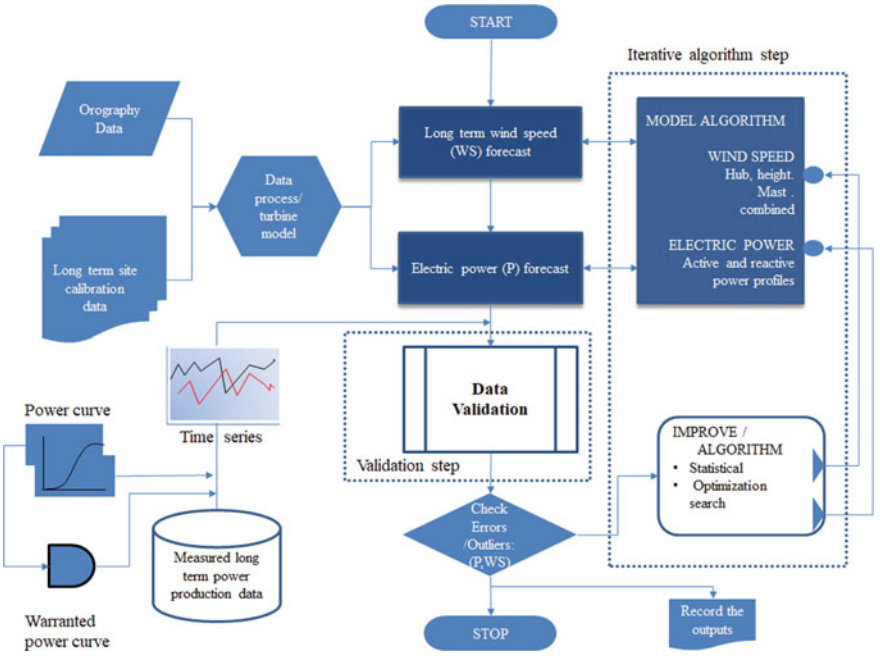

Fig. 14.5 Schematic for iterative numerical prediction algorithm used in wind farm data analysis

2% reduction in energy production. Also, the recommended distance for placement of test anemometers is between two and six rotor diameters and at a height equal to hub height of wind turbine. Further, another factor which affects energy yield from a turbine is surface roughness condition of blade during operation which varies due to accumulation of dirt, ice, rime or insects. This leads to blade degradation and accounts between 3 and 5% reduction in annual energy yield from a wind turbine.

It must be noted that as average distance of met mast in a site increases, the uncertainty of wind speed measurement also increases. According to IEC 61400-12-1, the gross errors in the annual energy yield would double for every 1% increase in wind speed measurement error. Overall, about 10–15% reduction of gross energy yield from wind park can be possible due to the above factors considered (Wind energy, The facts, Part-I; Technology 2014).

14.6 Mathematical Relation Between Scale and Shape Factor

In this section, the relationship between the shape and scale factor using Weibull distribution is derived using Eqs. (14.32) to (14.38)

$$f(V) = k \cdot \frac{V^{k-1}}{c^k} \cdot e^{-\left(\frac{V}{c}\right)^k} \tag{14.32}$$

$$\overline{V} = \int_0^\infty V f(V) dV \tag{14.33}$$

$$\text{Let} \left(\frac{V}{c}\right)^k = y \tag{14.34.1}$$

$$V = c y^{\frac{1}{k}} \tag{14.34.2}$$

$$dV = \frac{c}{k} y^{\frac{1}{k}-1} dy \tag{14.34.3}$$

Substituting Eqs. (14.32) and (14.34.1, 14.34.2, 14.34.3) in Eq. (14.33) we get

$$\overline{V} = c \int_0^\infty e^{-y} y^{\frac{1}{k}} dy \tag{14.35}$$

After rearrangement Eq. (14.35) reduces to Eq. (14.36) and using identity of Eq. (14.37.1) we obtain Eq. (14.37.2)

$$\overline{V} = c \int_0^\infty e^{-y} y^{1+\frac{1}{k}-1} dy \tag{14.36}$$

$$\int_0^\infty e^{-y} y^{1+\frac{1}{k}-1} dy = \Gamma\left(1 + \frac{1}{k}\right) \tag{14.37.1}$$

$$\overline{V} = c\Gamma\left(1 + \frac{1}{k}\right) \tag{14.37.2}$$

$$c = \frac{\overline{V}}{\Gamma\left(1 + \frac{1}{k}\right)} \tag{14.38}$$

where k and c are shape and scale parameters, respectively, and $\overline{V}$ is wind velocity. $f(V)$ is probability density function. One can obtain scale factor using gamma function when $\overline{V}$ annual mean wind speed at site is known. (Bhadra et al. 2010)

Equation (14.38) is used to estimate the energy for a given period based on scale and shape factors. From Eq. (14.38) one can estimate the wind power density (WPD) at a site using the following relation

$$WPD = \frac{1}{2}\rho c^3 \Gamma\left(1 + \frac{3}{k}\right) \tag{14.39}$$

Equation (14.39) is obtained by substituting the value of $\overline{V}$ in Eqs. (14.38) into (14.24). One can note that wind power density is a function of scale factor and shape factor which varies according to site location (Saxena and Rao 2016). More detailed analysis of energy yield assessment is presented in Sect. 14.7.3.

14.7 Results and Discussion

14.7.1 Turbine Efficiency and Dynamics

As mentioned in Sect. 14.4, the performance of a HAWT is dependent on aerodynamic lift and drag force coefficients which to a large extent depend on geometric and structural properties of blade. The C_p of turbine is computed for variable range of lift to drag coefficient ratios. For a turbine operating in wind farm array, the expanding helical wake behind the rotor affects the net power production and thus efficiency. The highest efficiency is obtained when wakes are spaced equidistant behind the rotor. Figure 14.6 depicts the influence of force coefficient ratio (L/D) on efficiency of wind turbine rotor element. The value of this ratio changes with the type of airfoils, operating tip speed ratio of rotor and surface roughness profiles of blade. Typically, thin airfoils such as NACA 4 digit and 6 series are slender wing elements present in outer annular ring while thick airfoils are present in inner annular ring (Ladson and Brooks 1996). The maximum blade lift usually varies in a range between 30 and 80% of blade span. From Fig. 14.6 it can be observed that as L/D ratios are increased the C_p values also tend to increase steadily for moderate to high values of λ between 4 and 10. For tip speed ratio (TSR) of 8, a step change in L/D from 40 to 120 showed

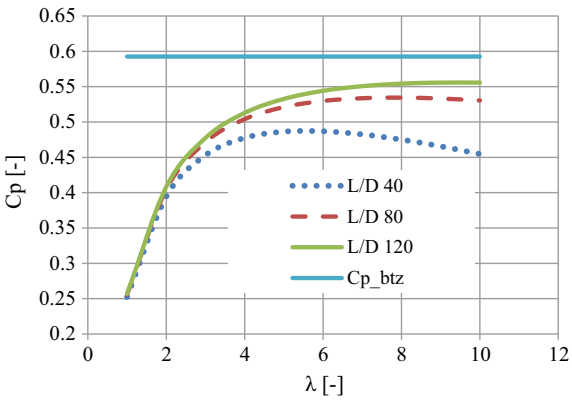

Fig. 14.6 Computed mechanical power coefficient for different L/D ratios of wind turbine rotor element

a 17% increase in C_p value. This increasing trend is seen for TSR values between 6 and 10. The horizontal straight line shows the maximum power coefficient obtained considering no wake rotation and possible only for idealized wind turbine.

However, from Fig. 14.7 for a given L/D ratio, significant change in C_p value is found for tip speed ratios less than 6 at different rotor solidity values. It corresponds to ~50% increase in C_p when three blades are present in turbine than when only one blade is used in rotor. During the Cp calculation, tip losses which account for aerodynamic power loss have been considered so that computed values can be compared readily with values obtained using measured data. Figure 14.8 shows the angle of attack (AOA) for varying tip speed ratios. It can be seen that for low tip speed ratios, the AOA are found as high as 50° towards the blade root region. As the tip speed ratio is increased, the AOA is reduced to as low as 5° and affect the maximum lift coefficient on the blade. In comparison to wind turbine rotors, commercial aircraft wings operate at low incidence angles at remarkably high Reynolds number.

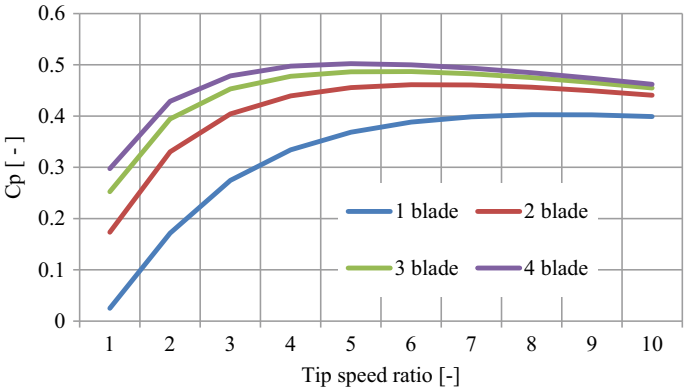

Fig. 14.7 Mechanical C_p computed for a turbine consisting of 1–4 blades with a L/D = 40 and considering tip loss correction, but no drag

Fig. 14.8 Angle of attack distribution for a blade length of 17 m at varying tip speed ratios

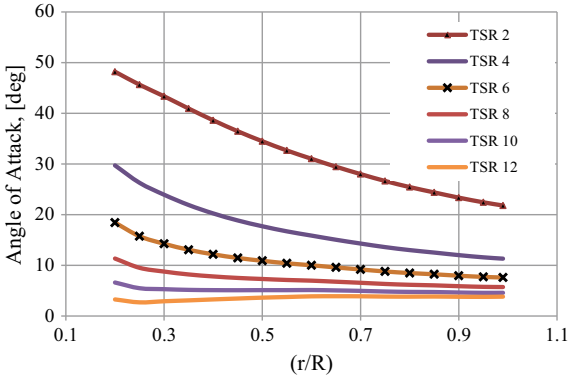

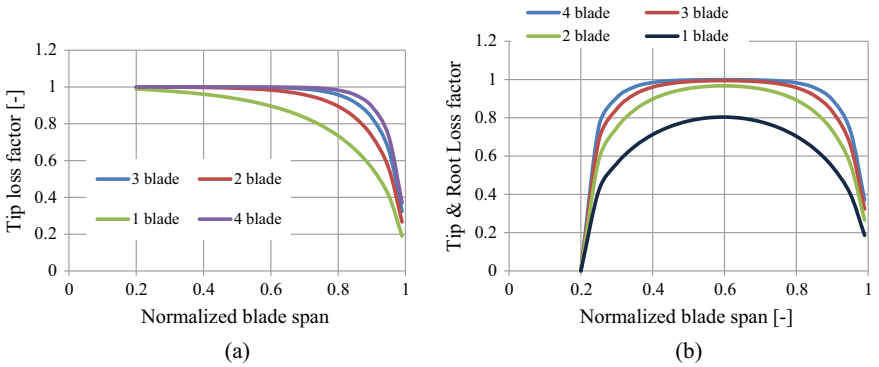

Fig. 14.9 **a** Prandtl tip vortex loss correction factor for varying number of blades, **b** combined with hub vortex loss

It can be noted that vortices are formed at tip and root regions that develops as cyclical wake screw and propagate leeward side of the rotor (Snel and Schepers 1995). Also, the magnitude of axial-induced velocity varies with the wake distance downstream and the thrust coefficient. When the wake expands downstream of the rotor, flow becomes more turbulent, and a higher velocity deficit is experienced by downstream turbine. As a result, higher thrust coefficient far downstream in the wake is produced and causes increase in fatigue loads on blade.

Figure 14.9a shows the Prandtl tip loss correction factor evaluated for one, two, three and four blades of a turbine. It is apparent that tip losses are higher towards the inboard region of blade where the thickness to chord ratio for airfoils is high but reduce eventually to a finite non-zero value. This trend is true for all horizontal axis turbines irrespective of number of blades. The total wake loss factor is depicted in Fig. 14.9b. Both wake and hub velocity deficits are computed at 20% of total blade length. The maximum wake loss was observed between 40 and 80% of length of blade for incremental blade count. It must be noted that tip vortices increase with varying aspect ratio of blade. As the aspect ratio is reduced to less than one, the maximum lift coefficient of a given blade section would increase. However, for low to moderate Reynolds number flows, vortices can be formed quickly due to flow separation which occurs at the leading edge of blade (Genc et al. 2016). The axial induction factor variation along the blade span is shown for the cases local to blade and azimuthal directions which seem to diverge at the tip as depicted in Fig. 14.10.

As discussed in Sect. 14.3, the axial induction factor a at rotor disk is indicator of velocity deficit used to test BEMT. This value also varies according to the blade azimuth orientation. Figure 14.11 shows the computed values for a at various span positions of blade for azimuth angles between 0° and 360°. It can be seen for span position of 0.99 R, a value fluctuates between 0.14 and 0.65. In the present study, the reference blade azimuth angles for three blades are assumed to be located at 90°, 210° and 330° with respect to the tower axis (Chaudhry et al. 2014; Arramach et al. 2017).

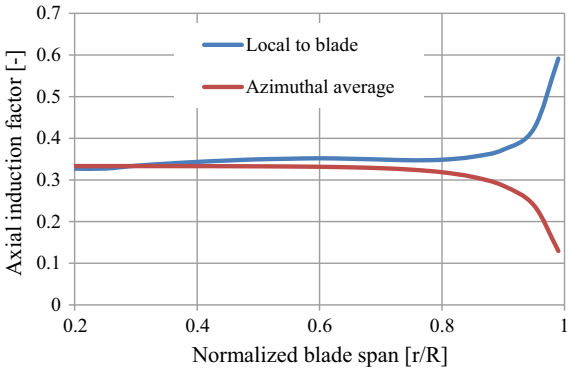

Fig. 14.10 Distribution of axial induction factor values local to blade and in rotor azimuth averaged conditions for a blade length of 17 m

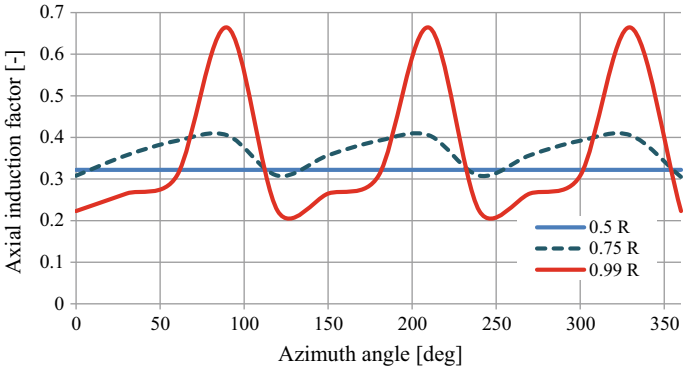

Fig. 14.11 Computed axial induction factors at 0.5R, 0.75R and 0.99R locations along blade span of length 17 m for various rotor blade azimuth angles

However, it can also be seen that for span positions of 0.75R, the maximum values of axial induction factor reached 0.43 only. Similarly, for span position of 0.5R the axial induction factor is constant at 0.5. For outboard span positions, the value of a fluctuates rapidly when the blades pass the tower structure and produce higher velocity deficit in wake. It can be said that for small size wind turbines with high twist distribution, the angle of attack and Reynolds number dependency affect the boundary layer flow behaviour. At high values of AOA, the span-wise flow become turbulent and degenerates towards the tip region of blade forming vortices. The Reynolds number for blade lengths of order of 17 m vary from low to moderate values, viz. 3×10^5 to 8×10^5. In contrast for large size turbines, with rotor diameters above 80 m equipped with high thickness to chord ratios, Reynolds numbers up to 3 million are possible.

Figure 14.12 shows that Glauert's momentum theory predicts higher power coefficient values up to 50% even for moderate to high yaw angles. For such angles, wake expansion and rotation effect behind the rotor increases faster (Bhadra et al. 2010;

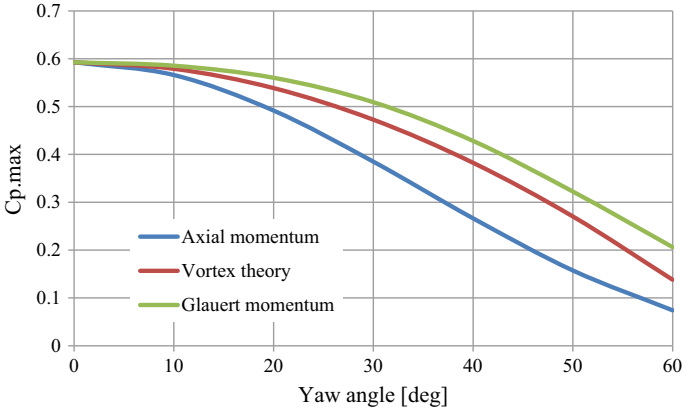

Fig. 14.12 Comparison of maximum mechanical power coefficient using axial momentum, vortex cylinder and Glauert theories for varying yaw angles

Hansen 2010). This approach is less conservative in nature as the wake expansion behind the rotor introduces significant increase in the axial thrust coefficient on the rotor. Also, it can be observed that axial momentum theory predicts 10 to 15% lower maximum power coefficient compared to vortex cylinder theory and Glauert theories. The C_{pmax} predicted according to axial momentum, Glauert's momentum and vortex cylinder model of yawed actuator disc is according to Eq. (3.90), Eq. (3.106) and Eq. (112) given in Bossanyi et al. (2005). As mentioned in Sect. 14.3, the magnitude of aerodynamic forces varies along the blade span which can be resolved in normal and tangential directions to rotor plane. The normal force per unit length at a given blade section increases towards the tip and contributes to thrust while tangential force per unit length contributes to torque. Typically, the tangential force per unit length is approximately 2–3 times the normal force per unit length (Bhargava et al. 2020; Krishna et al. 2018). In Fig. 14.13, a comparison of thrust coefficient evaluated according to Eq. (14.10) for varying yaw angles of turbine is depicted. As the yaw angle is increased, the axial force on blade decreases. For yawed rotor the wake becomes turbulent for higher yaw angles. Notice that thrust coefficient is reduced for axial induction factors beyond 0.5 where the momentum theory becomes invalid. One reason is that for large wake expansions, the axial-induced velocity reaches a limiting value relative to wind direction flow. For un-yawed rotor the change in wind velocity in wake of turbine is found to be half its initial value (Bossanyi et al. 2005). From Fig. 14.14a thrust coefficient obtained from BEM theory is valid until C_T reached a maximum value of 1 at axial induction factor of 0.5. Beyond this value the thrust coefficient predicted by BEM theory is invalid and starts reducing even when the axial induction factor a increases and reaches zero when the value of a is 1. For axial induction factor greater than 0.5, the wake expansion behind the rotor occurs rapidly and becomes highly turbulent for which predicted thrust coefficient is not accurate. This behavior is not observed in case of Glauert thrust coefficient correction, which increases up to value of 2. This shows that Glauerts proposition is

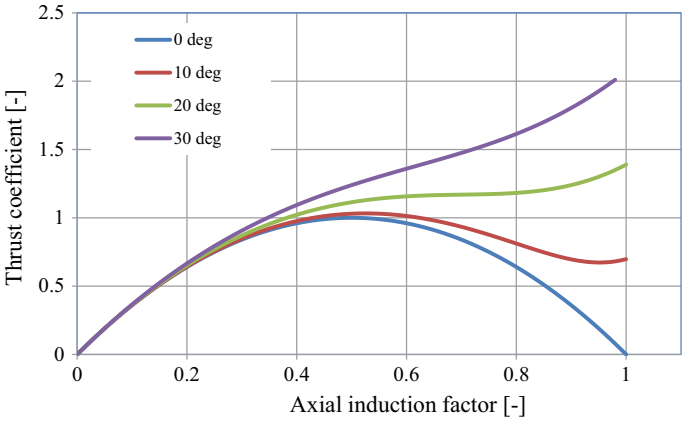

Fig. 14.13 Comparison of thrust coefficients for zero and non-zero yaw angles at different axial induction factors using BEM theory

less conservative in the prediction of thrust coefficient compared to vortex cylinder and axial momentum theories. To overcome these drawbacks, corrections for axial induction factor and thrust coefficient were proposed by Spera et al. (1979), Marshal and Buhl (2005), and Aagaard Madsen et al. (2012). The axial induction factor and thrust coefficient corrections are expressed using Eqs. (40) to (46) given in El-Okda (2015).

Figure 14.14a also compares the thrust coefficient values obtained from experiment (Lock et al. 1925) with the Buhls and Wilson–Walker correction factors. It must be noted that correction factors for thrust coefficient are evaluated when the Prandtl tip loss factor for rotor blades $F = 1$. Similarly, Fig. 14.14b, d represent the comparison of BEM predicted thrust coefficient with the correction factors proposed by Glauert, Buhl and Wilson–Walker and validated them using the experiment's obtained values. As the tip loss factor, F reduced the maximum thrust coefficient predicted by BEM theory which varied from 1 to 0.5. It can be seen that peak values for Glauert and Wilson–Walker correction factors also reduced for axial induction factors greater than 0.5. Also, the experiment data obtained by Lock et al. (1925) agreed well with thrust coefficient for axial induction factor more than 0.5 (Lock et al. 1925; Marshal and Buhl 2005). It can be noticed that Glauert's correction factor shows a discontinuity for values of $a > 0.4$ while Wilson correction factor is a tangent line to the BEMT curve and show discontinuity for $a > 0.2$. In contrast, Buhl correction factor is a continuous curve throughout the whole range of axial induction factor between 0 and 1. The discontinuity indicates aerodynamic instability when the BEMT produces invalid results.

Figure 14.15 shows that maximum power extraction ability increases towards the outboard of blade based on Eqs. (3.72) and (3.73) given in Bossanyi et al. (2005). Considering the Prandtl tip loss on the blade, the aerodynamic power extracted reduced to zero towards the tip of blade. In contrast, without tip loss correction,

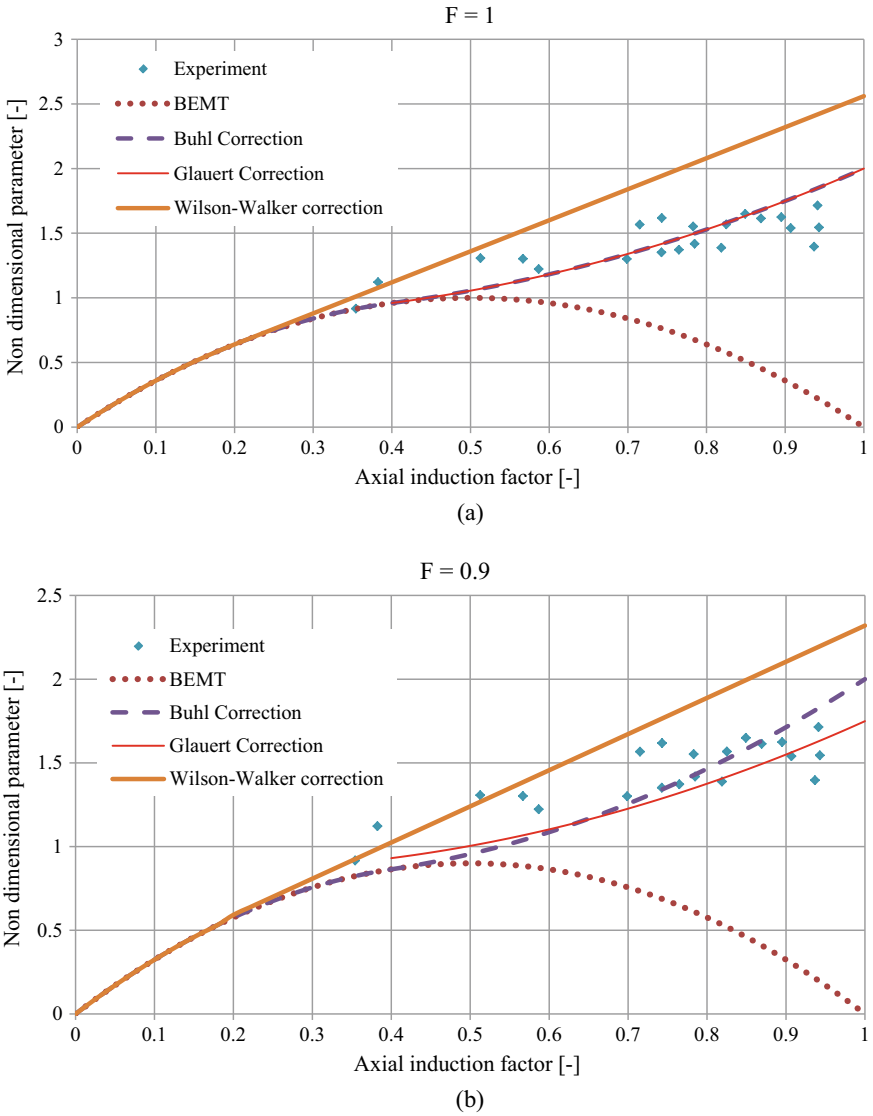

Fig. 14.14 Computed thrust coefficient using BEMT and Glauert, Buhl and Wilson–Walker correction factors and validated with experiment data for **a** $F = 1$, **b** for $F = 0.9$, **c** for $F = 0.7$, **d** for $F = 0.5$

the energetic flow continues to propagate if flow remains attached below the stall angle of attack; therefore, power extraction ability continues to increase.

Figure 14.16a, b show the aerodynamic forces per unit span length on the 47 and 17 m blades in normal (F_n) and tangential (F_t) directions of the rotor plane. The aerodynamic forces have been computed using BEMT including Prandtl tip

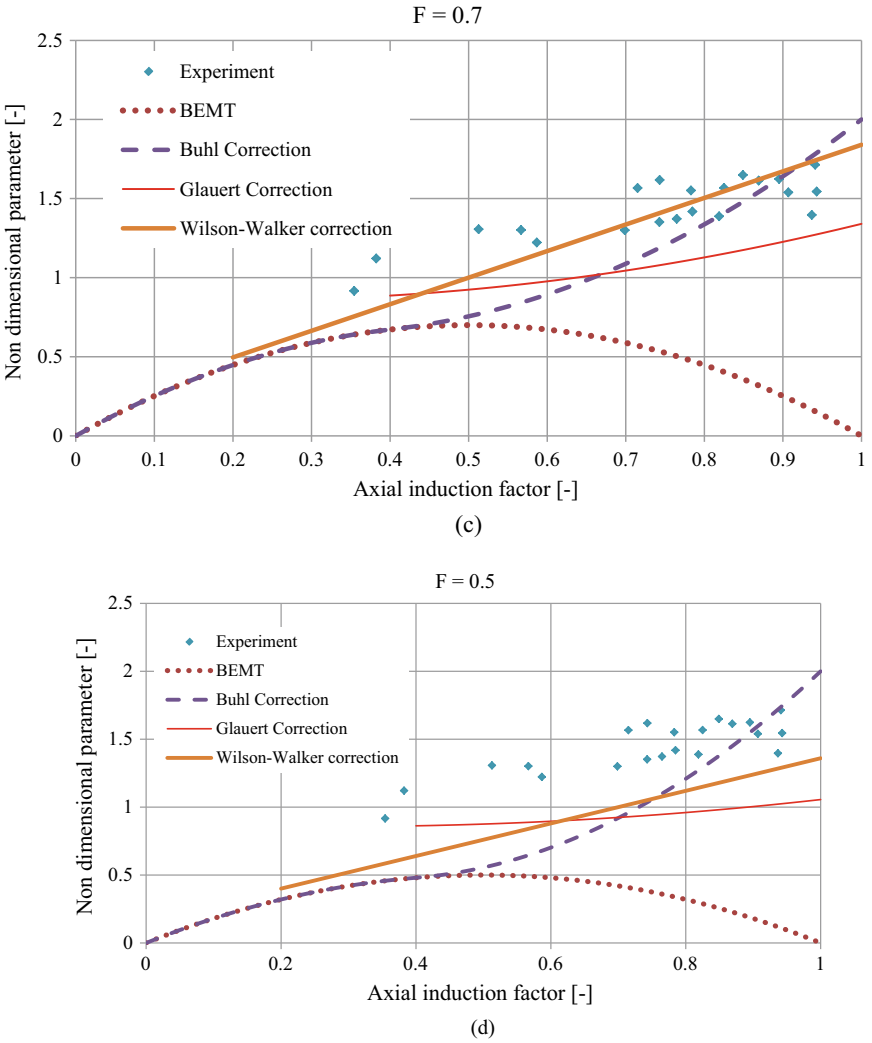

Fig. 14.14 (continued)

correction factor at wind speed of 12 m/s and 0° yaw. The forces can be seen to increase linearly towards the outboard region of blade but reduce near the tip. For 47 m blade, the maximum axial and tangential forces of 2889 N/m and 536 N/m are found while for 17 m blade it is 862 N/m and 171 N/m, respectively. This shows that BEMT predicts non-linear aerodynamic forces accurately for wide range of hub height wind speeds. Further, the magnitude of axial force on the rotor is nearly six times higher than the tangential force. In comparison to 47 m blade, force on the 17 m blade length varied by more than three times. This implies that loading on rotor is also increased significantly around rated wind speeds. Also, for pitch-controlled

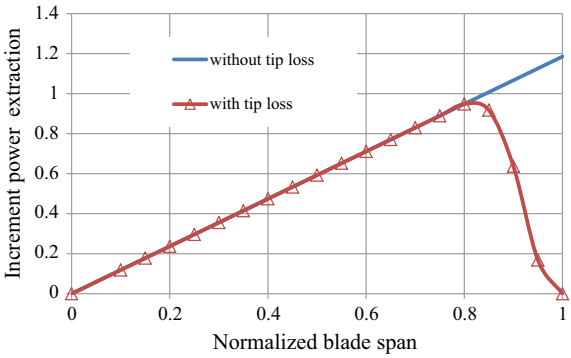

Fig. 14.15 Incremental power extracted with and without tip loss factors along blade span having a length of 17 m

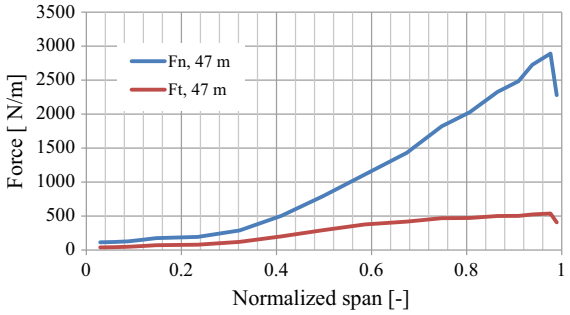

(a)

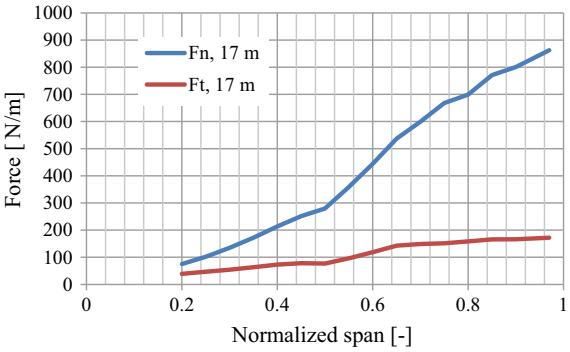

(b)

Fig. 14.16 BEM computed normal (F_n) and tangential (F_t) aerodynamic forces per unit span at wind speed of 12 m/s and 0° yaw using BEMT for **a** 47 m blade. **b** 17 m blade

turbines at near and above rated wind speed operation, loading on rotor in the axial direction increases heavily due to continuous blade pitching action to optimize the aerodynamic power of the turbine. Specifically, the flap-wise loads on blade vary dramatically compared to edge-wise load in response to the unsteady wind speeds.

14.7.2 Power Curve Assessment and Efficiency

The annual energy production from a turbine operating in wind farm can be predicted using long-term mean wind speed. At a given site, power curve modelling is an essential tool to estimate energy production from a wind turbine. Stochastic and deterministic methods can be used to develop power curve models to determine a relation between non-linear power outputs and wind speed at a site. Advanced power curve models utilize higher order polynomial models involving power coefficients (Teyabeen et al. 2017). The power output varies with wind bounded by regions known as cut-in wind speed at which the power is supplied to grid usually when the wind velocity is in the range of 2.5 and 5 m/s. The rated wind speed is expected when the machine delivers its nominal or nameplate capacity of electric power to grid, and finally cut-out wind speed when the generator is disconnected from the grid due to capacity constraints. Since instantaneous wind speed at a site is highly stochastic, it can be approximated using probabilistic function for accurate prediction of energy yield. Also, analytical methods such as measure correlate and predict (MCP) techniques are fairly accurate for estimating long-term wind speed data that trends at potential site. Based on IEC 61400-12-1 regulations for power curve measurements wind speed, direction and electrical power quantities are essential. Further measurements require air density, pressure, temperature and turbulence intensity corrections according to the bin averaging procedures. To evaluate turbulence intensity, standard deviation of longitudinal wind speed data is necessary. Using the short-term data for wind speed and direction, the turbulence intensity cannot be known accurately because binning method does not take account of data for the maximum hub height averaged wind speed over long term. Table 14.4 indicates the comparison of power curves for the machine at two different site air densities 1.115 and 1.225 kg/m^3 along with turbulence intensity. The TI values decay for above rated wind speeds but remain strongest between cut-in and rated wind speed operation. The standard deviation of wind speed did not vary appreciably between lower threshold and nominal wind velocities; however, for above nominal wind velocities, the deviation can be seen higher due to fewer 10 min averaged data present in each bin. It can be noted that a deviation between measured and manufacturer power data is often due to change in atmospheric variables, e.g. density of air. Therefore, for power curve performance air density correction is done based on IEC 61400-12 procedures mentioned in Bossanyi et al. (2005).

From Fig. 14.17a, the bin averaged power curves at two different air densities 1.225 and 1.115 kg/m^3 are illustrated along with measured power data between cut-in and rated wind speeds. It can be seen that data points that are scattered near cut-in wind speed are non-linear and show an offset with respect to both power curves. The power curve in red color is obtained at site air density of 1.115 kg/m^3. The manufacturer power curve is shown in green color line and taken from technical data specifications of model turbine. The comparison shows that bin averaged power curves fit the power data well in upper quartile range. It also indicates that distortion due to binning and occurrence of power errors are likely when power curves are derived from 10-min

Table 14.4 C_p obtained for 95 m rotor using wind speed frequency distribution

	Power coefficient (–)		Wind speed		Turbulence Intensity
WS, m/s	Standard	Measured	Frequency count	Stdev	%
1	0.000	−0.298	7	0.151	15.12
2	0.000	−0.019	47	0.261	13.04
3	0.000	0.099	182	0.269	8.95
4	0.174	0.164	355	0.287	7.18
5	0.351	0.332	363	0.293	5.86
6	0.409	0.386	359	0.296	4.93
7	0.424	0.405	476	0.289	4.12
8	0.430	0.411	579	0.286	3.57
9	0.423	0.404	687	0.289	3.21
10	0.402	0.389	496	0.294	2.94
11	0.361	0.353	454	0.301	2.74
12	0.311	0.301	261	0.286	2.38
13	0.251	0.245	108	0.263	2.03
14	0.201	0.196	21	0.311	2.22
15	0.163	0.160	10	0.300	2.00
16	0.135	0.132	3	0.321	2.01

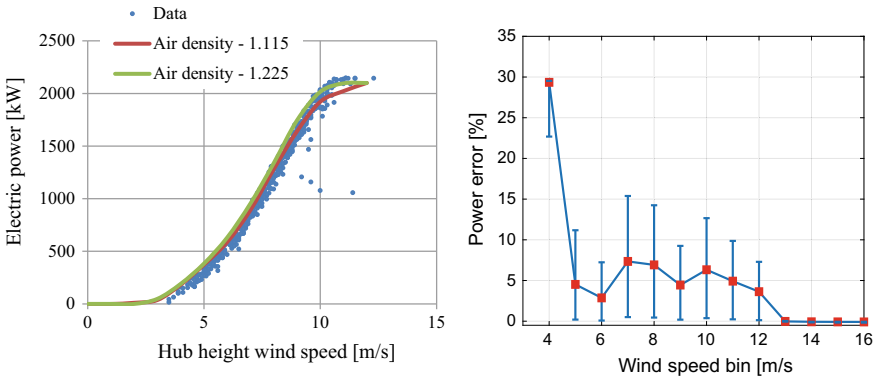

Fig. 14.17 **a** Power curve of manufacturer at air density of 1.225 kg/m^3 and observed data at 1.115 kg/m^3. **b** Graph of electric power error in % at air densities of 1.225 and 1.115 kg/m^3

averaged data. As the rated wind speed is approached, the linearity trend observed for data is lower compared to bin averaged power curves. It can also be observed that few outliers for power data are found at near rated wind speeds ~10 m/s. This can be due to distortion of bin data or from power curtailment operation imposed by controller to reduce the mechanical loads on the blade. Figure 14.17b illustrates the electric power error between cut-in and rated wind speeds. Maximum power error of 29% is seen near cut-in wind speed with a low uncertainty. However, power error reduced to 5% at 5 m/s wind speed bin and increased to 7% at the rated wind speed. The blue color bar shows the uncertainty in the power error which is highest for 7 and 8 m/s wind speed bins. The present bin analysis is based on the 10 min bin averaged data which does not capture the dynamics of power curve accurately. So according to Milan et al. (2014) to overcome this limitation, combined stochastic and mathematical modelling of power curve at sampling frequency of 1 Hz would be useful for accurate power predictions (Milan et al. 2014). The annual energy production from wind turbine can be monitored with the help of central data control and acquisition software to log the operational data continuously. Following are main turbine operating conditions.

- Machine is started using sequential controller steps.
- Machine is connected to grid to be able to supply power.
- Machine is stopped whenever external conditions and uncertain events occur. For example 50-year gust, loss of grid.
- Grid curtailment mode according to network grid conditions.
- Rotor freewheeling when there is no wind enough for power production to grid.

Figure 14.18 shows the blade pitch angle between minimum and nominal wind velocities. It can be seen that rotor speed increase steadily soon after cut-in wind speed and remains constant up to rated wind speed. During this period, the blade pitch angle varied between 0° and 5° where aerodynamic power extraction is maximized by controller algorithm (Chaudhry et al. 2014). So, for below rated wind speeds one

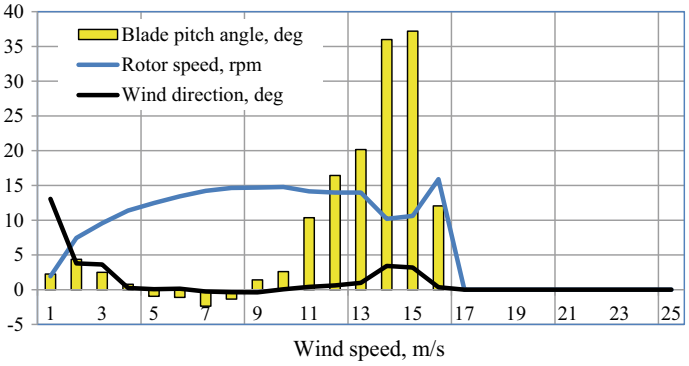

Fig. 14.18 Bin averaged values for blade pitch angle, rotor speed and wind direction at different wind speeds for pitch-controlled turbine

must note that optimum turbine performance is regulated continuously to track the wind. Also, for below rated wind speed the tip speed is found as 79.08 m/s when TSR varied between 4 and 8. In case of turbines with fixed speed, this value reaches set point for specific wind velocity; however, for machines which can produce power at different rotor speeds, it is varied in such a way that $C_{p\max}$ is obtained. A feedback control loop ensures to optimize the C_p even for low wind regimes. Also, for a turbine in which power is regulated by pitch movement of the blade with its leading edge into wind, a phenomenon known as *pitch to feather* occurs for above rated wind speed operation. Pitch to feather action reduces the unsteady aerodynamic lift on blades which lowers the fatigue loads on rotor. In contrast, for stall-controlled turbines operating at above rated wind speeds, the blade experiences dynamic stall on its suction side for high angles of attack. This phenomenon also occurs in a non-linear manner which tends to increase fatigue loads on turbine components. So, the controller regulates power output from turbine by turning the trailing edge into wind and this process otherwise known as *pitch to stall.* Since bin averaging is applied to the 10-min measured data set for each wind speed between cut-in and cut-out, the power errors for individual bin are corrected by applying standard deviation to the average values. A maximum power value of 2141 kW can be found for above rated wind speed bins. The standard deviation for the bin averaged values of wind speed and electric power increased due to the low data samples used for averaging.

Figure 14.19 shows the 10 min bin values for thrust coefficient for below rated wind speed operation or for high tip speed ratio. It varied between 0.9 and 0.98 with fluctuations seen close to cut-in wind speed. This value is turbine specific which cannot be compared with others operating in a wind farm array. Similarly, for power coefficient it varies between 0.32 and 0.44, respectively.

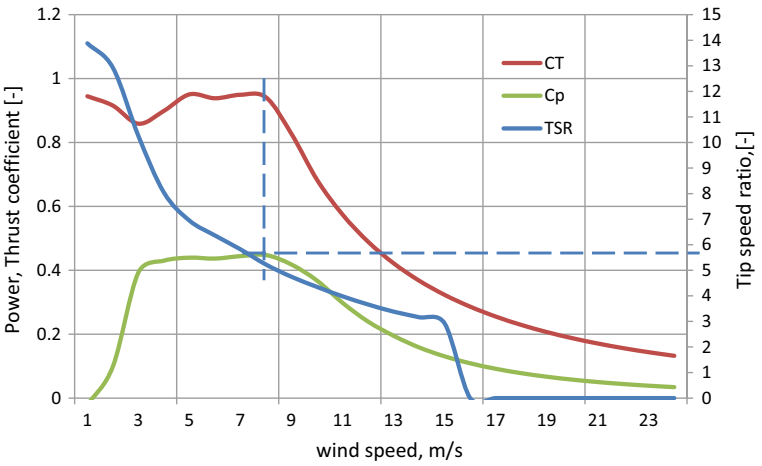

Fig. 14.19 Thrust and power coefficients for 95 m turbine rotor and tip speed ratio between cut-in and cut-out wind speeds

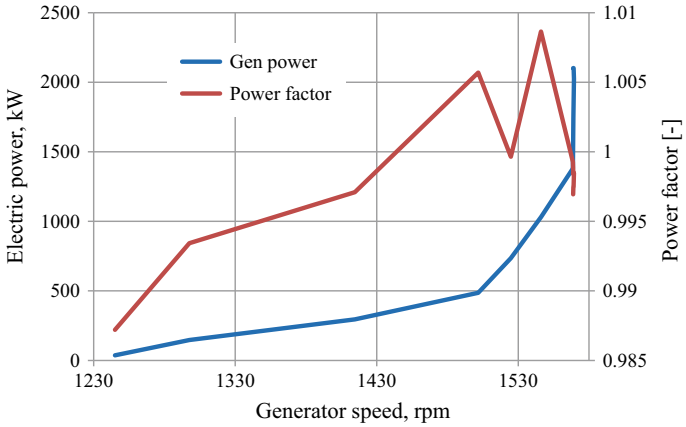

Fig. 14.20 Comparison of generated power and power factor versus speed characteristic for variable pitch control turbine

To know wind speed and directions, an anemometer and wind vane installed on a met mast at height equal to hub height located few rotor diameters away from turbine are required. It can be noted that readings from sensors located on the nacelle may not be accurate. Therefore, corrections have been applied to power curve as described in Sect. 14.5. The power produced by any turbine can be controlled using the measured rotor speed and blade pitch angle sensors located in hub controller. This signal is sent to main controller via a feedback loop to compare and track the set-point values of rotor speed and blade pitch angle. To measure the generator, speed proximity inductive sensor is used. The sensor data is continuously monitored and can be used to determine the operating state of turbine. It can be observed from Fig. 14.20 that rated power for generator is ~1569 rpm and the power factor value is ~1. For below rated wind speed operation, the generator speeds vary between 1250 and 1500 rpm, and ramp-up is observed. When the rotor speed is operating near rated values, the generator speed remains nearly constant after which the generator torque output is kept constant by controller once it reaches the rated value. When approaching synchronous speeds of the generator a non-linear behaviour in power production can be seen. It can also be seen that power factor also known as cosϕ fluctuates near rated generator speed, exact reason of which could be attributed to grid stability and turbine control procedures near rated wind speed (Bhadra et al. 2010).

Figure 14.21 shows a comparison of power coefficient, obtained using bin averaging method at various λ values and for blade pitch of 0°. The graph showing the power coefficient value was obtained using the empirical relation using Eqs. (14.30) and (14.31) with following values for constants, $c_1 = 0.4176$, $c_2 = 135$, $c_3 = 2.1$, $c_4 = 9.3$, $c_5 = 15.7$ and $c_6 = 0.0088$, respectively. For TSR less than 7, C_p predicted using bin method and model agreed within 1% demonstrating that for low blade pitch angles between 0° and 5° constants in Eqs. (14.30) and (14.31) produce expected

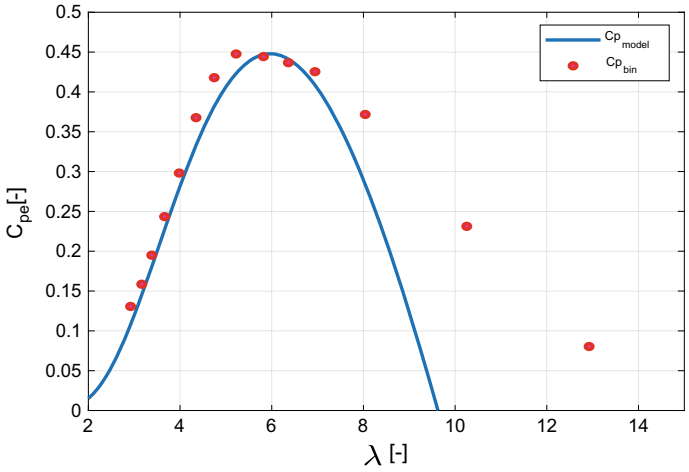

Fig. 14.21 Computed power coefficient for various tip speed ratios using bin averaged data and model output at 0° blade pitch angle

power output with a high fidelity. On the other hand, for TSR values greater than 7, divergence for C_p values can be observed clearly. Apparently, a difference of ~25% can be seen at high tip speed ratios. One reason for this difference is attached to quantity of data used in the binning procedures. It can be noted that design tip speed ratio predicted by model agreed well within 1% of value obtained from measured data.

The time-series history for low-speed shaft torque, power and wind velocity are shown in Fig. 14.22. It can be observed from data that turbine experienced high wind conditions for about 1.5 days. However, power and low speed shaft moment

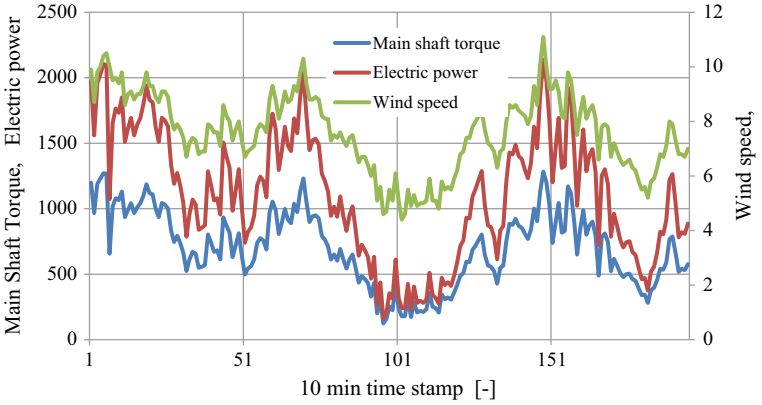

Fig. 14.22 Time-series history of low-speed shaft torque, kN-m, electric power, kW and wind velocity, m/s for period of 34 h

are 201 kW and 124.3 kN-m, between time stamp values of 90 and 110, as result of direction change of wind. At any given location, direction of wind velocity can be obtained using a wind vane. The nacelle controller computes the directional turns of nacelle and prevents the turbine from failure. In some turbines, the transformer room is integrated into nacelle to reduce the cabling costs and to prevent them from breaking during yaw. For wind speeds close to cut-in values, the low-speed shaft torque and power fluctuate. For the sampled data, it was found to be 160 kW and 124.3 kN-m. However, near rated wind speeds between 11 m/s and 12 m/s the generator produces ~2100 kW and ~1285 kN-m. For measured data, total axial rotor force of 323.6 kN, turning moment of 1289 kN-m and power of 2140.1 kW for the turbine are apparent.

14.7.3 Energy Yield Prediction

In this section, the energy yield prediction from manufacturer and bin averaged power curves are demonstrated (Directory of Indian Wind Power 2012). From the manufacturer power curve table, the minimum wind velocity for the turbine is 3.5 m/s while nominal speed is 11 m/s. These values are recorded at air density of 1.225 kg/m^3 and at standard temperature and pressure conditions. But the minimum and maximum wind velocities vary according to size of turbine. As the rotor diameter becomes larger, the power extraction ability of rotor increases. To predict energy yield from a machine, the long-term wind speed modelling is essential. For meteorology and wind turbine applications a Weibull probability density function is most suitable for analysis of long-term wind speed frequency distribution at a place (Sohoni et al. 2016). Fundamentally it consists of two random variables, viz. shape and scale factors for predicting the wind speed frequency. The shape factor considers geographic features of terrain, while the scale factor indicates the long-term wind speed for a location. The likelihood of velocity occurrence and corresponding energy production data for a given period shows the likelihood of energy generation from a machine. Turbine designers and wind resource analysts use such information for sizing and design of turbine components as well as in site prospecting. Also, the net power from wind farm is calculated using measured data for any period based on active and reactive values of power. It has been found to be 0.77 and 0.067 GWh and resultant energy for duration of ~742 h is found to be 0.701 GWh. Furthermore, the difference in energy yield can be accounted to several factors as mentioned in Sect. 14.5. According to Ehrmann et al. (2017), blade surface roughness affects the wind turbine performance by reducing the lift to drag ratio of rotor blades. For surface roughness height ranging from 140 μm to 1 mm on blade, an estimated 2–3% loss in annual energy production is possible due to 40% reduction of lift to drag ratio. The Weibull probability density function for various shape factors at a scale factor of 8.5 m/s is shown in Fig. 14.22.

One can observe that as annual average wind velocity increases, the likelihood of energy capture increases at a location. Further, from the occurrence of bin averaged air velocity are higher for annual mean wind speeds of 8.5 m/s and 7.5 m/s, respectively.

Figures 14.23 and 14.24 show the influence of shape factor and scale factor on likelihood of occurrence of a given wind speed at a given location. Figure 14.23 shows that the probability density function is skewed towards left and has amplitude that range between 0.08 to 0.1 for wind speeds lower than 7 m/s. The monthly shape factor range between 1.25 and 2.0. However, as the shape factor is increased beyond 2 the wind speed likelihood increased in amplitude for wind speeds between 7 and 10 m/s. On the other hand, from Fig. 14.24, as scale factor is reduced from 8.5 to 7.5 m/s the amplitude of density function varied from 0.114 to 0.1 without appreciable change. One can notice the tail of distribution in both Figs. 14.23 and 14.24 is similar and approach same limiting values with amplitudes that range between 0 and 0.02 for higher values of wind speeds. However, in Fig. 14.24 the tails appear to be fatter as the shape factor is reduced. This indicates that for a given scale factor, the likelihood of energy extraction at such wind speed increased by ~1%. Figure 14.25

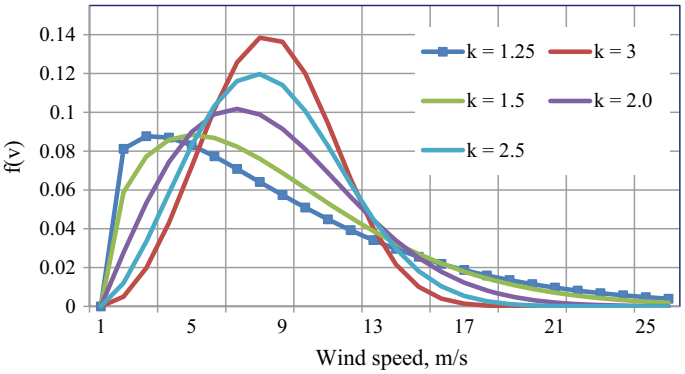

Fig. 14.23 Weibull wind speed probability density function at different shape factors for given scale factor of 8.5 m/s

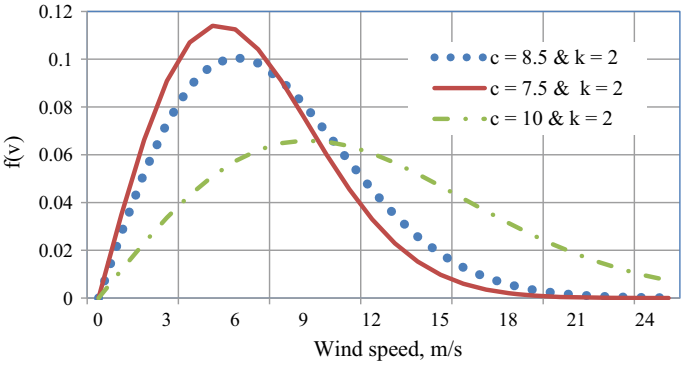

Fig. 14.24 Weibull wind speed probability density function at different scale factors at constant shape factor of 2

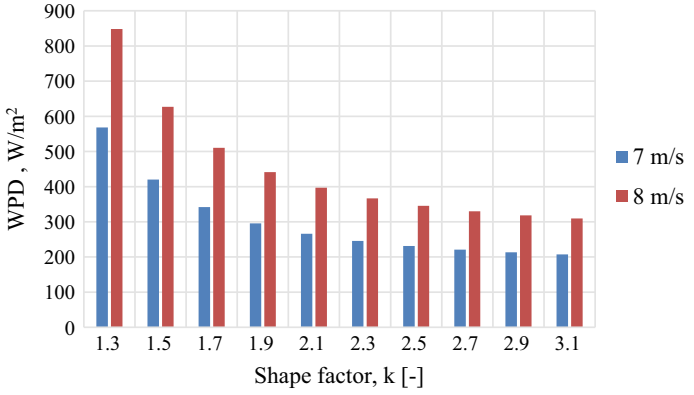

Fig. 14.25 Graph of annual wind power density for different annual scale and shape factors obtained using two-parameter Weibull distribution

shows the annual wind power density (WPD) computed for different shape and scale factors using Eq. (14.39) presented in Sect. 14.6. Wind power density is a quantity which shows the kinetic energy available in the wind at any specified location and is usually calculated at specific height above ground. On the other hand, specific power indicates amount of aerodynamic power that can be extracted by turbine over a finite swept area of rotor. A geographic area can be categorized according to wind power density and are known as wind zones. According to Directory of Indian Wind Power (2012), there are seven wind zones with distinct mean wind speed values which range from 6 to 10 m/s. So, wind power density at a site could be estimated from Weibull distribution parameters, viz. scale and shape factor as discussed earlier in this section. Practical values for wind power density are measured at specific height above the ground level. Typically met mast installed at 100 m or 50 m above ground level are used as reference for measuring wind power density values. It can be noted that for annual scale factor of 7 m/s the WPD varied from 568 to 201 W/m^2 as the annual shape factor is increased from 1.3 to 3.1. This shows that high values of shape factor showed a negative effect on wind power density which implies lower energy available in wind for power production. However, when the annual scale factor is increased from 7 m/s to 8 m/s the annual wind power density is increased by ~ 49%. It must be noted that computed values are based on the theoretical estimates of two parameter Weibull distribution. Hence, Weibull distribution is a useful tool in site prospecting and wind resource assessment.

Table 14.5 shows the comparison of monthly Weibull energy GWh, estimated using manufacturer and measured power curves for different scale and shape factors. The analysis used the excel WEIBULL function which accepts two input parameters to estimate the approximate number of hours for bin averaged wind speeds. Theoretical hours data and power data for the corresponding bin are obtained from standard power curve to forecast energy output. Weibull energy variation was found to be ~33% when shape factor changed from 1.3 to 2.1 while a ~13% when scale

Table 14.5 Weibull energy yield comparison using manufacturer and measured power curves of 95 m rotor at air densities 1.115 and 1.225 kg/m^3

Power curve type	Weibull hours	Scale factor	Shape factor	Energy (GWh)
				Weibull
MSRD	712.1	9.5	2.1	0.652
STRD	712.1	9.5	2.1	0.725
MSRD	641.3	9.2	1.3	0.466
STRD	642.1	9.2	1.3	0.510
MSRD	624.4	8.4	2.1	0.567
STRD	624.3	8.4	2.1	0.634
MSRD	416.1	7.77	1.1	0.379
STRD	416.2	7.77	1.1	0.416

factor changed from 7.7 to 9.5 m/s. The predicted values for energy yield are found when the turbine is not under any major shutdown events. In practice O&M includes downtime factors which account up to 2–4% reduction in the annual yield production.

From Table 14.6 the annual energy yield for turbine showed an increase of 16% when the annual scale factor is varied from 7.5 to 8.5 m/s. For rotor diameter of 36 m, the expected annual production is 0.835 GWh when the annual scale factor is 7.5 m/s and 0.977 GWh when the scale factor is increased to 8.5 m/s. The estimated Weibull energy is obtained using standard power curves for the turbines measured at 1.225 kg/m^3. When the rotor diameter is increased by 3 times, the expected annual energy output from the turbines increase by ~6 times. A large rotor diameter implies higher amount of aerodynamic power extracted per swept area of turbine. However, one must note that power extraction ability depends on the operating state and power curve characteristics of turbine as discussed in Sect. 14.7.2. Hence, performance and energy yield prediction of wind turbines can be done effectively through simulation of high-fidelity theoretical aerodynamic models, as well as application of advanced empirical or analytical methods.

Table 14.6 Weibull annual energy yield computed for turbines with 95 and 36 m rotor diameter at scale factors of 8.5, 7.5 m/s and shape factor of 1.4

Rotor diameter (m)	Power curve type	Annual Weibull hours	Shape factor	Scale factor	Energy (GWh)
					Weibull
95	Standard	8545.2	1.4	7.5	6.31
36	Standard	8547.1	1.4	7.5	0.835
95	Standard	8525.4	1.4	8.5	7.34
36	Standard	8521.3	1.4	8.5	0.977

14.8 Conclusions

- In this paper, we studied blade element momentum theory and its improvements to find operating characteristics of HAWT rotors. Various design factors such as tip speed ratio, rotor diameter, blade count and pitch angle, L/D ratios were investigated using sampled operational data. Power and thrust coefficients are key parameters to measure turbine efficiency. Bin data analysis showed that peak thrust and power coefficient values were found to be 0.945 and 0.44 for wind turbine with 95 m rotor diameter. BEM analysis revealed that turbines with small rotor diameters exhibited aerodynamic forces which were three to four times lower compared to megawatt scale turbines.
- Induction variable along rotor axis and thrust corrections proposed by Glauert, Buhl and Wilson–Walker showed good agreements with those predicted from BEMT for values less than 0.5; however, thrust coefficient predicted using conventional BEMT agreed well with experiment data when the induction variable is greater than 0.5. For all correction models, the maximum values for thrust coefficients reduced as the combined tip and hub loss factors are reduced from 1 to 0.5.
- With increase in blade count, the wake losses from tip of rotor were found to be lower. The maximum aerodynamic power from a blade becomes higher towards the outboard of blade. When the lift to drag ratio is changed from 40 to 120, it resulted in 17% improvement of aerodynamic efficiency of turbine. Hence, it can be concluded that increasing the rotor solidity and lift to drag ratios will increase the aerodynamic power extraction ability.
- A method for performing data binning to analyze SCADA operational data using a pseudocode has been presented. The code was designed to extract power, torque and thrust coefficients for given wind speed data. Results of binning procedure showed that maximum power error of 28% is found at cut-in wind speed due to power outliers present in bin data. An empirical relation for predicting C_p using TSR and blade pitch angle was proposed to verify the accuracy of the predictions. The model predictions were validated using the bin averaged power coefficient data. The results for power coefficient agreed within 1% of the measured data for tip speed ratios less than 7 but found to disagree between 7 and 10.
- Long-term energy yield using two-parameter Weibull distribution requires different shape and scale factors, and bin-wise frequency distribution of wind velocity. In contrast to fixed speed stall-controlled machines, the maximum power production is not constant for variable speed machines between minimum and nominal wind velocities for which the tip speed ratios varied between 5 and 7.

References

Aagaard Madsen H, Riziotis V, Zahle F, Hansen MOL, Snel H, Grasso F, Larsen TJ, Politis E, Rasmussen F (2012) Blade element momentum modelling of inflow with shear in comparison with advanced model results. Wind Energy 15(1):63–81

Andrew TL, Flay RGJ (1999) Compliant blades for wind turbines. IPENZ Trans 26:7–12. https://doi.org/10.1260/0309524001495369

Arramach J, Boutammachte N, Bouatem A, Al Mers A (2017) Prediction of the wind turbine performance by using a modified BEM theory with an advanced brake state model. Energy Procedia 118:149–157. https://doi.org/10.1016/j.egypro.2017.07.033

Astolfi D, Castellani F, Bechetti M, Lombardi A, Terzi L (2020) Wind turbine systematic yaw error: operation data, analysis techniques for detecting it and assessing its performance impact. Energies 13:2351. https://doi.org/10.3390/en13092351

Bhadra SN, Kastha D, Banerjee S (2010) Wind electrical systems. Oxford Education, New Delhi

Bhargava V, Kasuba S, Maddula SP, Donepudi J, Akhtar MDK, Padhy C, Chinta HP, Sekhar CS, Dwivedi YD (2020) A case study of wind turbine loads and performance using steady state analysis of BEM. Int J Sustain Energy 40:22–40. https://doi.org/10.1080/14786451.2020.1787411

Bontempo R, Manna M (2019) Verification of the axial momentum theory for propellers with a uniform load distribution. Int J Turbomachinery Propulsion Power 4:8. https://doi.org/10.3390/ijtpp4020008

Bossanyi E, Sharpe D, Jenkins N, Burton T (2005) Wind energy handbook. Wiley, London

Chaudhry U, Mondal P, Tripathy P, Nayak SK, Saha UK (2014) Modeling and optimal design of small HAWT blades for analyzing the starting torque behavior. In: 18th National power systems conference, Guwahati, India, pp 1–6. https://doi.org/10.1109/NPSC.2014.7103886

Corrigan JJ, Schillings JJ (1994) Empirical model for stall delay due to rotation. In: American Helicopter Society aeromechanics specialists conference, San Francisco CA

De Vries O (1979) Fluid dynamic aspects of wind energy conversion. AGARD report, AG-243, Chapter 4

Directory of Indian Wind Power. Consolidated Energy Consultants, Bhopal. India (2012)

Djojodihardjo H, Abdul Hamid MF, Jaafar AA, Basri S, Romli FI, Mustapha F, Mohd Rafie AS, Abdul Majid DLA (2013) Computational study on the aerodynamic performance of wind turbine airfoil fitted with Coanda Jet. J Renew Energy 2013. https://doi.org/10.1155/2013/839319

Ehrmann RS, Wilcox B, White EB, Maniaci DC (2017) Effect of surface roughness on wind turbine performance. Sandia report, SAND2017-10669. https://doi.org/10.2172/1596202

El-Okda MY (2015) Design methods of horizontal axis wind turbine rotor blades. Int J Ind Electron Drives 2:135–150

Emblemsvag J (2020) On the levelised cost of energy of wind farms. Int J Sustain Energy 39:700–718. https://doi.org/10.1080/14786451.2020.1753742

Froude (1885). https://en.wikipedia.org/wiki/Momentum_theory#:~:text=In%20fluid%20dynamics%2C%20momentum%20theory,Robert%20Edmund%20Froude%20(1889)

Gasch R, Twele J (2012) Wind power plants, fundamentals, design, construction and operation, 2nd edn. Berlin

Genc SM, Ozkan G, Acikel HH, Kiris MS, Yildiz R (2016) Effect of tip vortices on flow over NACA4412 aerofoil with different aspect ratios. https://doi.org/10.1051/epjconf/201611402027

Germanisher L (2007) Guideline for certification of wind turbines, Edition 2003 with supplement 2004, Reprints Hamburg

Glauert H (1948) The elements of airfoil and airscrew theory, 2nd edn. Cambridge University Press

Goudarzi N, Zhu WD (2013) A review on the development of wind turbine generators across the world. Int J Dyn Control 1:192–202. https://doi.org/10.1007/s40435-013-0016-y

Hansen MOL (2010) Aerodynamics of wind turbines. James & James, London, UK

Heier S (1998) Grid integration of wind energy conversion systems. Wiley, Kassel, Germany

Javaherchi T, Antheaume S, Aliseda A (2014) Hierarchical methodology for the numerical simulation of the flow field around and in the wake of horizontal axis wind turbines: rotating reference frame, blade element method and actuator disk model. J Wind Eng 38:181–201

Jiang H, Cheng Z, Zhao Y (2012) Torque limit of horizontal axis wind turbine. In: Proceedings of international conference mechanical engineering & materials sciences. MEMS. https://doi.org/10.2991/mems.2012.114

Jordan D et al (2019) Wind turbine technical report

Krishna JM, Bhargava V, Donepudi J (2018) BEM prediction of wind turbine operation and performance. Int J Renew Energy Res 8:1962–1973

Ladson CL, Brooks CW (1996) Computer program to obtain ordinates for NACA airfoil. Langley. Research Center, document ID: 19970008124, Hampton, Virginia

Lock CNH, Bateman H, Townsend HCH (1925) An extension of the vortex theory of airscrews with applications to airscrews of small pitch including experimental results No. 1014. Aeronautical research committee reports and memoranda, London, Her Majesty Stationery Office

Mansberger L (2016) Thermodynamic wind turbine model addendum. Mansberger Aircraft Inc., Fortworth, Texas, USA

Manwell JF, McGowan JG, Rogers AL (2009) Wind energy explained, theory, design and application, 2nd edn, Wiley, London, UK

Marshal L, Buhl Jr (2005) A new empirical relationship between thrust coefficient and induction factor for the turbulent wind mill state, NREL Technical report, NREL/TP-500-36834

Mikkelsen R, Sorensen JN, Ivanell S, Henningson D (2009) Analysis of numerically generated wake structures. Wind Energy 12:63–80. https://doi.org/10.1002/we.285

Milan P, Wachter M, Peinke J (2014) Stochastic modelling and performance monitoring of wind farm power production. J Renew Sustain Energy. https://doi.org/10.1063/1.4880235

Numerical Manufacturing and Design Tool, NuMAD. https://energy.sandia.gov/programs/renewable-energy/wind-power/rotor-innovation/numerical-manufacturing-and-design-tool-numad/

Ouakki Y, Arbaoui A (2020) Accurate loads and velocities on low solidity wind turbines using an improved blade element momentum model. Wind Energy Sci. https://doi.org/10.5194/wes-2020-43

Power performance testing, 2nd edn, Expert group study on recommended practices for wind turbine testing and evaluation (1990)

Prandtl (1935). https://en.wikipedia.org/wiki/Blade_element_theory

Ragheb M, Ragheb AM (2011) Wind turbine theory—the Betz equation and optimal rotor tip speed ratio. In: Fundamental and advanced topics in wind power. IntechOpen

Saxena BK, Rao KVS (2016) Estimation of wind power density at a wind farm site located in western Rajasthan region of India. In: International conference on emerging trends in engineering, science and technology, ICETEST

Sebastian PB, Francesco P, Joseph S, David M, Alessandro B, Oliver CP (2019) Is the blade element momentum theory overestimating wind turbine loads?—a comparison with a lifting line free vortex wake method. Wind Energy Sci 5:721–743. https://doi.org/10.5194/wes-5-721-2020

Shen WJ, Mikkelsen R, Sorensen JN, Bak C (2005) Tip loss corrections for wind turbine computations. J Wind Energy 8:457–475. https://doi.org/10.1002/we.153

Sherry M, Sheridan J, Jacono DL (2013) Characterization of a horizontal axis wind turbine's tip and root vortices. Exp Fluids 54:1417. https://doi.org/10.1007/s00348-012-1417-y

Snel H, Schepers JG (1995) Joint investigation of dynamic inflow effects and implementation of an engineering method. Energy Research Centre Netherlands, ECN–C-94-107

Sohoni V, Gupta SC, Nema RK (2016) A critical review on wind turbine power curve modelling techniques and their applications in wind-based energy systems. J Energy 2016:1–18. https://doi.org/10.1155/2016/8519785

Spera DA, Viterna LA, Richards TR, Neustadter HE (1979) Preliminary analysis of performance and loads data from the 2-Megawatt MOD-1 wind turbine generator. In: 4th Biennial conference and workshop on wind energy conversion systems. Department of energy, Washington D.C, U.S

Strangfeld C, Rumsey CL, Muller Vahl H, Greenblatt D, Nayeri CN, Paschereit CO (2015) Unsteady thick airfoil aerodynamics: experiments, computation and theory. In: 45th AIAA fluid dynamics conference, Dallas, Texas, USA. https://doi.org/10.2514/6.2015-3071

Tangler JL, Selig MS (1997) An evaluation of an empirical model for stall delay due to rotation for HAWTs. In: Proceedings windpower, Austin TX, pp 87–96

Teyabeen AA, Akkari FR, Jwaid AE (2017) Power curve modelling for wind turbines. In: 19th international conference on modelling and simulation

Vermeer LJ, Sorensen JN, Crespo A (2003) Wind turbine wake aerodynamics. Prog Aerosp Sci 39:467–510. https://doi.org/10.1016/S0376-0421(03)00078-2

Wind energy, The facts, Part-I; Technology. Garrad Hassan and Partners Ltd, Bristol, UK (2014)

Xu G, Sankar LN (2002) Application of a viscous flow methodology to the NREL phase-IV rotor. In: ASME wind energy symposium, Reno, AIAA-2002-0030, pp 83–93